ARTICLES
https://doi.org/10.1038/s41590-018-0254-4
nature immunology

TCF-1 and HEB cooperate to establish the epigenetic and transcription profiles of CD4$^+$CD8$^+$ thymocytes

Akinola Olumide Emmanuel[1], Stephen Arnovitz[1], Leila Haghi[1], Priya S. Mathur[1], Soumi Mondal[1], Jasmin Quandt[1], Michael K. Okoreeh[1], Mark Maienschein-Cline[2], Khashayarsha Khazaie[3], Marei Dose[1*] and Fotini Gounari[1*]

Thymocyte development requires a complex orchestration of multiple transcription factors. Ablating either TCF-1 or HEB in CD4$^+$CD8$^+$ thymocytes elicits similar developmental outcomes including increased proliferation, decreased survival, and fewer late *Tcra* rearrangements. Here, we provide a mechanistic explanation for these similarities by showing that TCF-1 and HEB share ~7,000 DNA-binding sites genome wide and promote chromatin accessibility. The binding of both TCF-1 and HEB was required at these shared sites for epigenetic and transcriptional gene regulation. Binding of TCF-1 and HEB to their conserved motifs in the enhancer regions of genes associated with T cell differentiation promoted their expression. Binding to sites lacking conserved motifs in the promoter regions of cell-cycle-associated genes limited proliferation. TCF-1 displaced nucleosomes, allowing for chromatin accessibility. Importantly, TCF-1 inhibited Notch signaling and consequently protected HEB from Notch-mediated proteasomal degradation. Thus, TCF-1 shifts nucleosomes and safeguards HEB, thereby enabling their cooperation in establishing the epigenetic and transcription profiles of CD4$^+$CD8$^+$ thymocytes.

The CD4$^+$CD8$^+$ double-positive (DP) stage of T cell development encompasses critical developmental checkpoints, including rearrangement of the T cell antigen receptor (TCR) alpha (*Tcra*) locus, assembly of the αβ T cell receptor (αβTCR), and passage through thymic selection[1]. DP thymocytes arise from the proliferative double-negative (DN) 4 stage, which is controlled by cooperative pre-TCR and Notch signals[2]. Coordination among transcriptional regulators has been established for early stages of T cell development, in which Notch signals activate transcription of TCF-1 (encoded by *Tcf7*)[3,4] and GATA-3 (refs [5,6]), whereas Pu.1 regulates the binding-site choice of Runx1 and consequently the initiation of the T cell program[7–9]. Together, Notch, TCF-1, GATA-3, and Runx1 activate Bcl11b and seal the T cell fate[7,10]. T cell commitment in DN2 cells coincides with the upregulation of HEB (encoded by *Tcf12*), HEBAlt (HEB isoform), Runx1, Gfi1, and Ets1, which control subsequent T cell developmental stages[7,11–13]. Despite intense investigation, the orchestration of factors that regulate entry into and differentiation through the DP stages remains poorly understood.

Regulatory proteins implicated in the DP stages include TCF-1 (refs [14,15]) and HEB[16]. TCF-1, a member of the HMG-domain-containing Tcf/Lef family of transcriptional regulators, participates in complex transcriptional and epigenetic processes throughout T cell development. It interacts with β-catenin, thereby activating Wnt-target genes, and with Groucho, thereby silencing genes[17–19]. Although TCF-1 has intrinsic histone deacetylase activity[20], it also promotes chromatin accessibility and displaces nucleosomes at its binding sites[21]. The specific transcriptional and epigenetic functions of TCF-1 at the DP stage and its potential cooperation with other regulators remain unclear. HEB is a member of the E-protein family of transcription regulators, which are essential for the development of both B and T cells[22]. Through its helix–loop–helix domain, HEB can form homodimers as well as heterodimers with other E proteins, and consequently mediate positive and negative regulation of gene expression. Although HEB binds the acetyltransferase p300 (ref. [23]), its genome-wide chromatin-remodeling functions remain unclear.

In germline TCF-1-deficient thymocytes, the transition to the DP stage is impaired[14,15]. TCF-1 also controls the lifespan of DP thymocytes by upregulating the antiapoptotic protein Bcl-XL[24–26]. These shorter-lived DP thymocytes do not undergo distal *Tcra* gene rearrangements and therefore generate fewer natural killer T cells, which depend on these rearrangements[26]. Like TCF-1, HEB regulates the transition to the DP stage as well as the survival of DP thymocytes, and its deletion limits distal *Tcra* rearrangements and development of natural killer T cells[27]. After the DP stage, TCF-1 promotes the CD4$^+$ versus CD8$^+$ T cell fate[28]. HEB is also required for CD4$^+$ lineage commitment[29]. Thus, TCF-1 and HEB are fundamental in guiding thymocytes into and beyond the DP stages of development; however, whether they collaborate directly remains unclear.

Here, we found that most HEB-bound DNA sites genome wide were also bound by TCF-1. Cobinding of TCF-1 and HEB promoted chromatin accessibility, whereas TCF-1 predominantly limited nucleosome occupancy. TCF-1/HEB cobinding to their conserved motifs at the enhancers of genes involved in αβ T cell development correlated with transcriptional upregulation. In contrast, TCF-1 and HEB bound to sites that lacked their conserved motifs in the promoters of cell-cycle-associated genes, and ablation of either TCF-1 or HEB increased DP-thymocyte proliferation. Importantly, TCF-1 limited Notch signaling, which targets HEB for proteasomal degradation. Therefore, TCF-1 both enhances HEB protein stability and

[1]Department of Medicine, University of Chicago, Chicago, IL, USA. [2]Core for Research Informatics, University of Illinois at Chicago, Chicago, IL, USA. [3]Department of Immunology, Department of Surgery, Mayo Clinic, Rochester, MN, USA. *e-mail: mareidose0@gmail.com; fgounari@uchicago.edu

functionally cooperates with HEB in defining the epigenetic and transcriptional status of DP thymocytes.

Results

TCF-1 binding marks actively transcribed genes. We previously established, through chromatin immunoprecipitation and deep sequencing (ChIP–seq)[30,31] that in wild-type (WT) thymocytes, TCF-1 binds more than 16,000 sites genome wide. To identify regions of accessible chromatin in WT DP thymocytes, we performed the assay for transposase-accessible chromatin and deep sequencing (ATAC–seq). Alignment of the ATAC–seq results to our TCF-1 ChIP–seq data established that the chromatin surrounding the TCF-1 peaks in DP thymocytes was highly accessible (Fig. 1a). We also mapped the landscape of histone marks indicating poised/active (mono- and dimethylated histone H3 Lys4 (H3K4me1 and H3K4me2, respectively)), active (trimethylated H3 Lys 4 (H3K4me3) and acetylated H3 (H3ac and H3K27ac)), and repressed (trimethylated H3 Lys27 (H3K27me3)) chromatin proximal to TCF-1 sites. Of the TCF-1-bound sites, 43% were at active promoters enriched in H3K4me2/me3, H3ac, and H3K27ac histone marks as well as RNA polymerase (Pol) II, indicating transcriptional activity. Additionally, 24% of the TCF-1 bound sites were active enhancers, enriched in H3K4me1/me2, H3K27ac, and RNA Pol II, and 33% were poised enhancers marked by H3K4me1 but displaying low enrichment in H3K4me2 and H3K27ac, and lacking RNA Pol II (Fig. 1a–c). In contrast, TCF-1 binding rarely overlapped with the repressive H3K27me3 mark. Thus, TCF-1 occupies gene-regulatory regions enriched in marks of poised or active chromatin, thereby indicating that it directly regulates gene expression.

TCF-1 binding at open chromatin sites, enriched in RNA Pol II, suggested that its gene targets are actively transcribed. RNA-seq analysis of sorted WT DP thymocytes showed that the average expression of TCF-1-bound genes was higher than that of all expressed genes (Fig. 1d). In particular, genes bound by TCF-1 at promoters or at both promoter and enhancer regions showed significantly higher expression than genes bound only at active or poised enhancer regions. Thus, TCF-1 binds accessible regulatory regions of actively transcribed genes. Pathway enrichment analysis (http://www.metascape.org/) revealed that TCF-1 binding to promoters alone versus enhancers marks genes involved in distinct processes (Fig. 1e). Genes bound by TCF-1 only at promoter regions were involved in cell-cycle regulation. In contrast, TCF-1 binding at enhancers or both enhancer and promoter regions marked genes involved in T cell developmental processes. These findings suggest that TCF-1 differentially regulates these distinct processes through specific chromatin binding patterns, potentially in coordination with other factors.

TCF-1 shares binding sites with other lymphoid factors. To identify additional factors that might cooperate with TCF-1, we first analyzed TCF-1-binding sites for common motifs. TCF-1-bound sites were highly enriched in the conserved Tcf/Lef motif ($P=1\times10^{-1784}$). Additionally, motifs for Ikaros/Ets, Runx and basic helix–loop–helix domain–containing proteins were also significantly enriched at TCF-1-bound sites (Fig. 2a). These factors are essential during the transitions to the DP and single-positive stages of thymocyte development. Ikaros regulates differentiation from the $CD4^+CD8^{lo}$ postselected DP to the single-positive subsets, and its deletion predisposes mice to Notch-dependent thymic lymphomas[32,33]. Runx1 is involved in the progression from the DN to DP and single-positive stages and, with Runx3, is essential for $CD8^+$ lineage commitment[34]. Likewise, the basic helix–loop–helix domain–containing E2A and HEB regulate progression into, and exit from, the DP stage. Interestingly, HEB deficiency impairs thymic development in a manner akin to TCF-1 deficiency[16,27].

The involvement of these regulators in the DP stages of thymocyte development, and the enrichment of their motifs at TCF-1-bound sites, prompted us to examine whether their binding might overlap with that of TCF-1. We performed ChIP–seq for HEB and analyzed published ChIP–seq data for Ikaros[35], and Runx1 (ref. [36]) in WT thymocytes. We also performed ChIP–seq for Lef-1, which recognizes the same motif as TCF-1 and is thought to have redundant functions[37,38]. Even though Lef-1 occupied significantly fewer sites than TCF-1 (4,476/16,377), 79% of these sites (3,536) overlapped with TCF-1 (Fig. 2b). TCF-1-binding sites also overlapped with 53% of Ikaros-binding sites (2,018) and 47% of Runx1-binding sites (4,970). HEB shared the largest number of overlapping sites with TCF-1 (6,767), representing 55% of all HEB peaks. The peak summits of Ikaros, Runx1, and HEB in common sites with TCF-1 completely overlapped with TCF-1 peak summits, thus indicating that binding of these factors was centered on the same sequences (Fig. 2c–e).

We compared chromatin accessibility at sites bound by TCF-1 alone (6,883) with sites where TCF-1 overlapped with one other factor (5,482 sites; 63% with HEB, 28% with Runx1, and 9% with Ikaros), two factors (3,280 sites; 76% with HEB/Runx1 and 24% with HEB/Ikaros), or sites in which all four factors overlapped (732 sites). TCF-1 enrichment (peak score) and chromatin accessibility (ATAC–seq) progressively increased at sites where TCF-1 overlapped with additional factors, suggesting cooperativity (Fig. 2f). HEB was the preferential binding partner of TCF-1, sharing an extensive number of sites with TCF-1 as well as all multifactor TCF-1 sites. These findings led us to further investigate the functions of TCF-1 and HEB in DP thymocytes.

TCF-1 and HEB guide similar developmental processes. To understand the potential cooperative functions of TCF-1 and HEB, we compared thymocyte development after DP-specific deletion of either *Tcf7* or *Tcf12*. Conditional loss of TCF-1 or HEB, respectively, was accomplished with a *Cd4*-Cre transgene. Whereas *Cd4*-Cre*Tcf12*$^{fl/fl}$ mice (hereafter referred to as HEB deficient) exhibited sufficiently decreased HEB protein abundance in preselected DP thymocytes, the effective decrease in TCF-1 protein in the preselected DP thymocytes required crossing *Cd4*-Cre to *Tcf7*$^{fl/-}$ mice (hereafter referred to as TCF-1 deficient), as previously described[28]. Multiple studies have established that heterozygous TCF-1 deletion does not affect DP-thymocyte development[14,15,39]. TCF-1 or HEB deficiency mildly decreased thymic cellularity (Fig. 3a). In accordance with published observations[26,27], both TCF-1- and HEB-deficient DP thymocytes had greater apoptosis (annexin V^+), than did thymocytes from littermate controls (*Cd4*-Cre) (Fig. 3b). Additionally, qPCR showed that *Tcra* gene rearrangements were strongly biased for proximal and against distal Jα gene segments, in both TCF-1- and HEB-deficient DP thymocytes, probably because of the shorter lifespan of these cells (Fig. 3c). We further found that TCF-1- or HEB-deficient DP thymocytes were significantly more proliferative than thymocytes from littermate controls (Fig. 3d). Higher proliferation rates did not result from increased DP-blast thymocytes in *Cd4*-CreTcf7$^{fl/-}$ and *Cd4*-Cre*Tcf12*$^{fl/fl}$ thymi compared with WT thymi, because the fraction of $CD71^+FSC^{hi}$ blast DP cells did not significantly change (Supplementary Fig. 1). Thus, in addition to having overlapping genome-wide binding, TCF-1 and HEB regulate the same critical properties of DP thymocytes, suggesting that TCF-1 and HEB cooperatively regulate the DP stage of thymocyte development.

TCF-1/HEB shared sites mark genes involved in T cell development. Like TCF-1, HEB bound to accessible chromatin sites. The mean expression of HEB-bound genes was higher than that of all genes expressed in DP thymocytes. Genes bound by HEB at the promoters or both promoter and enhancer sites had the highest expression

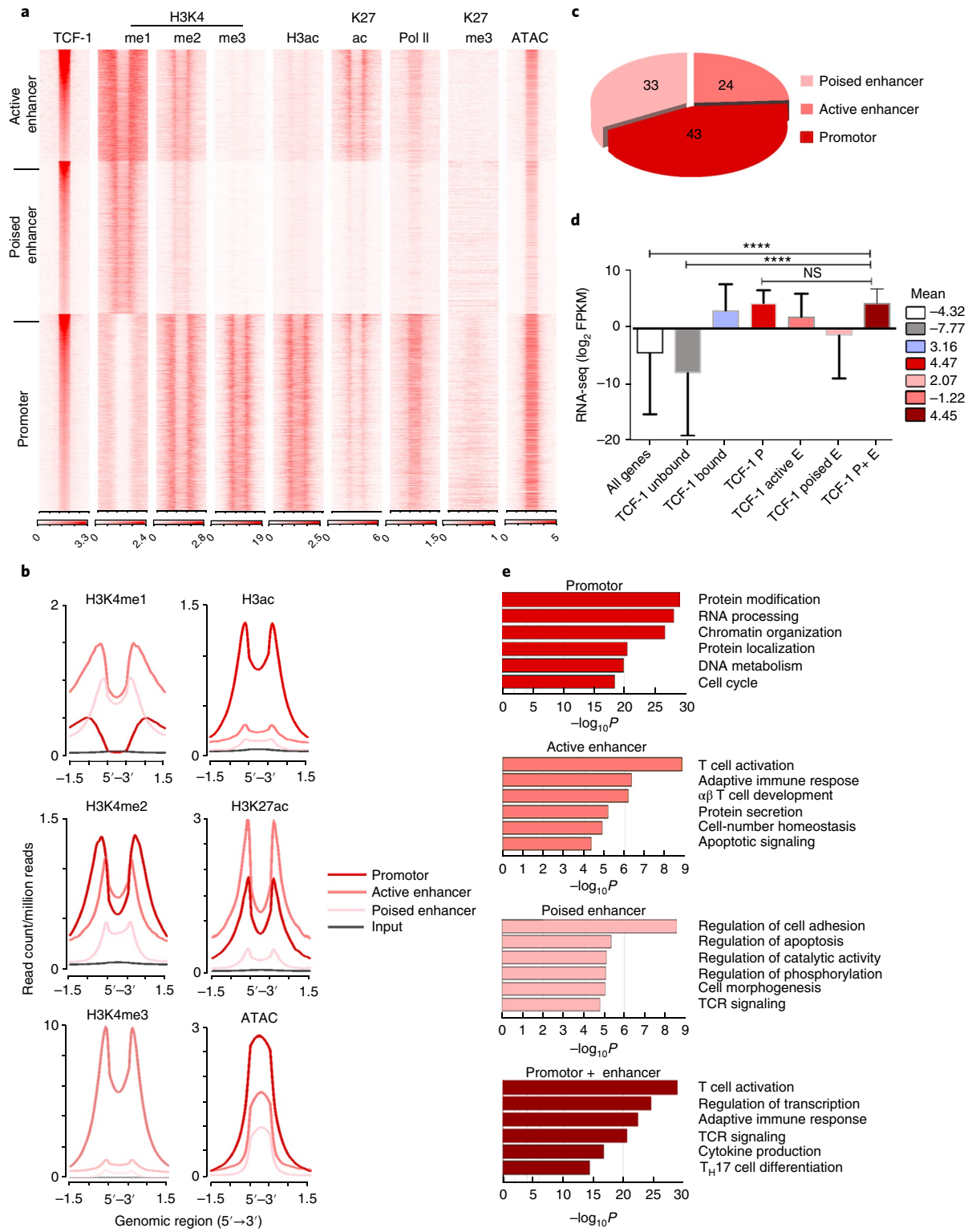

Fig. 1 | TCF-1 binds accessible chromatin of highly expressed genes. a, *K*-means-clustered heat map centered on TCF-1-binding sites (±1.5 kb) showing enrichment of the indicated histone modifications and RNA Pol II in WT thymocytes, and ATAC-seq in DP thymocytes. **b**, Comparative enrichment histograms of permissive histone modifications (H3ac, H3K4me1, H3K4me2, H3K4me3, and H3K27ac) and chromatin accessibility (ATAC-seq) at TCF-1-binding sites (±1.5 kb) in *K*-means clusters shown in **a**. **c**, Genomic distribution of TCF-1 peaks in WT thymocytes. **d**, Average expression in DP thymocytes of genes in the indicated groups. E, enhancer; P, promoter. Values are $\log_2$ fragments per kilobase of transcript per million mapped reads (FPKM), shown as mean with s.d. (****$P \leq 0.0001$, NS, not significant, Kruskal–Wallis test). (All genes, $n = 23{,}360$; TCF-1 unbound, $n = 18{,}384$; TCF-1 bound, $n = 4{,}976$; TCF-1 promoter, $n = 1{,}839$ genes; TCF-1 active enhancer, $n = 627$ genes; TCF-1 poised enhancer, $n = 920$ genes; TCF-1 promoter + enhancer, $n = 1{,}690$ genes). **e**, Functional pathways enriched in genes bound by TCF-1 in the indicated regions. (Active enhancer, $n = 527$ genes; poised enhancer, $n = 920$ genes; promoter, $n = 1{,}839$ genes; promoter + enhancer, $n = 1{,}690$ genes). Pathways and statistical enrichment were determined by Metascape (http://www.metascape.org/).

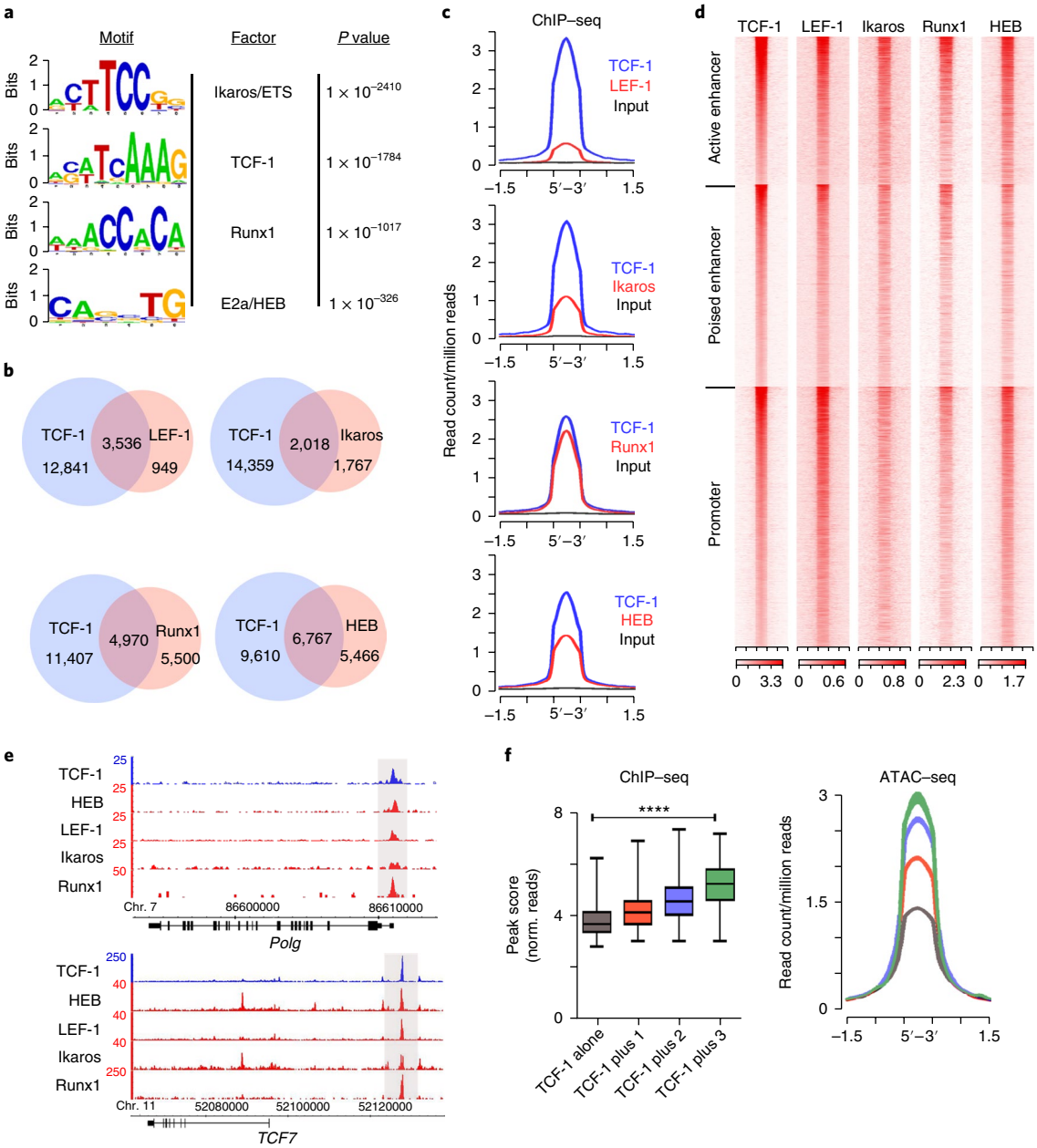

Fig. 2 | TCF-1 binding overlaps with LEF-1, HEB, Runx1, and Ikaros binding. a, De novo transcription-factor-binding motif analysis (HOMER) of TCF-1-binding sites in WT thymocytes. The most significantly enriched motifs and associated *P* values are shown. **b**, Venn diagrams of the numbers of overlapping peaks between TCF-1 and the indicated factors. **c**, Comparative enrichment histograms at overlapping DNA-binding sites of TCF-1 and the indicated factors (±1.5 kb). **d**, ChIP–seq heat map of the indicated factors centered on *K*-means-clustered TCF-1-binding sites (±1.5 kb). **e**, Representative multifactor-binding regions at the indicated loci (Integrated Genome Browser). ChIP–seq enrichment tracks are shown for TCF-1, HEB, LEF-1, Ikaros, and Runx1. Chr., chromosome. **f**, Box plots (left) and comparative accessibility histograms (right) depicting average $\log_2$ peak scores of TCF-1 binding at sites where TCF-1 binds alone or with one, two, or three factors. Norm., normalized. (****$P \leq 0.0001$, Kruskal–Wallis test; TCF-1 alone, $n = 6{,}883$ peaks; TCF-1 plus one, $n = 5{,}482$ peaks; TCF-1 plus two, $n = 3{,}280$ peaks; TCF-1 plus three, $n = 732$ peaks. Box plot: center line, median; box-plot limits, upper and lower quartiles; whiskers, 1.5× interquartile range.)

(Supplementary Fig. 2). To assess the potential cooperation between TCF-1 and HEB in DP thymocytes, we analyzed their overlapping binding sites. These sites were distributed to promoters as well as poised and active enhancers (Fig. 4a–d). The average expression of TCF-1/HEB cobound genes was significantly higher than that of all DP-thymocyte genes or genes uniquely bound by either TCF-1 or HEB (Fig. 4e). In particular, genes cobound by TCF-1 and HEB at both promoter and enhancer sequences showed the highest expression, followed by genes with binding at the promoter only.

Shared TCF-1 and HEB binding at promoters versus enhancers differed in several aspects. First, TCF-1 and HEB enrichment was highest at active enhancers (Fig. 4c). Second, TCF-1/HEB cobinding at promoters versus enhancers marked distinct groups of genes. Binding only to promoters marked genes involved in general cellular processes, such as cell division and the DNA-damage response (Fig. 4f and Supplementary Fig. 3). However, binding to enhancers or enhancers as well as promoters marked genes involved in T cell–specific processes, such as T cell activation and TCR signaling.

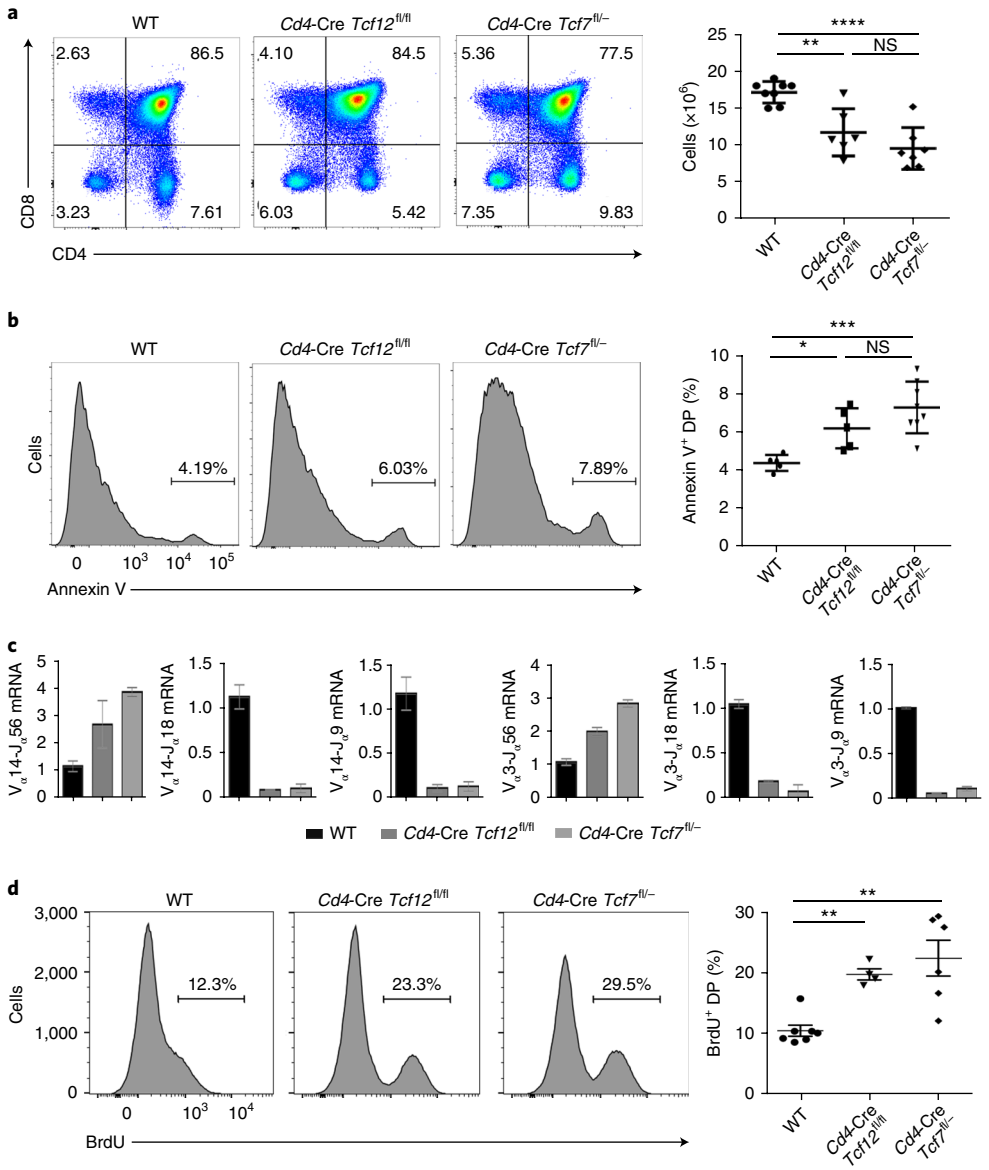

Fig. 3 | TCF-1 or HEB deficiency elicits similar developmental impairments. a, Flow cytometry of CD4 versus CD8 staining in WT, *Cd4*-Cre *Tcf12*$^{fl/fl}$, and *Cd4*-Cre *Tcf7*$^{fl/-}$ thymocytes from 6- to 8-week-old mice. Right, thymocyte numbers from the indicated mouse strains (WT, *n* (biologically independent samples) = 8; *Cd4*-Cre *Tcf12*$^{fl/fl}$, *n* = 6; *Cd4*-Cre *Tcf7*$^{fl/-}$, *n* = 7). (**$P \leq 0.01$, ****$P \leq 0.0001$, NS, not significant, ordinary one-way analysis of variance (ANOVA)). **b**, Histogram plots of annexin V staining of gated DP thymocytes in the indicated mouse strains. Right, cumulative plots of the fraction of annexin V$^+$ DP thymocytes in the indicated mouse strains (WT, *n* (biologically independent samples) = 5; *Cd4*-Cre *Tcf12*$^{fl/fl}$, *n* = 5; *Cd4*-Cre *Tcf7*$^{fl/-}$, *n* = 8). (*$P \leq 0.05$, ****$P \leq 0.0001$, ordinary one-way ANOVA). **c**, Quantitative PCR analysis of transcripts of $V_\alpha14$ and $V_\alpha3$ rearrangements to $J_\alpha56$, $J_\alpha18$, or $J_\alpha9$ segments in sorted DP thymocytes relative to the expression of C_α transcripts. Data are representative of two biologically independent experiments. Error bars, s.d. **d**, Histogram plots of bromodeoxyuridine (BrdU) staining in gated DP thymocytes in the indicated mouse strains. Right, cumulative plots of the fraction of BrdU$^+$ DP thymocytes (**$P \leq 0.01$, ordinary one-way ANOVA). (WT, *n* (biologically independent samples) = 6; *Cd4*-Cre *Tcf12*$^{fl/fl}$, *n* = 4; *Cd4*-Cre *Tcf7*$^{fl/-}$, *n* = 5).

This binding pattern resembled that observed for all TCF-1-bound sites (Fig. 3b–d). We further identified regions with extensive TCF-1 and HEB binding by using a rank-order super-cluster algorithm that stitches together adjacent transcription-factor peaks within 12.5-kb regions[40]. Of the 271 TCF-1 and 213 HEB super-clusters identified (Supplementary Fig. 4), 126 overlapped, and most were in enhancers, whereas only 11 were located in promoters. Overlapping super-clusters occurred mostly at the enhancers of genes involved in TCR signaling, recombination, and apoptosis, highlighting DP-thymocyte processes affected by ablation of TCF-1 or HEB. Thus, TCF-1/HEB cobinding to gene promoters versus enhancers identifies distinct processes. Independently deleting either protein functionally impairs these processes in DP thymocytes, suggesting that TCF-1 and HEB cooperatively regulate the transcriptional and/or epigenetic state of the associated genes.

TCF-1 and HEB promote chromatin accessibility at cobound sites. To determine the importance of the extensive binding overlap between TCF-1 and HEB, we assessed the binding of HEB in TCF-1-deficient DP thymocytes and of TCF-1 in HEB-deficient DP thymocytes by ChIP–seq (Fig. 5). Only 2,813 high-confidence ($P = 10 \times 10^{-5}$) HEB sites were identified in TCF-1-deficient thymocytes,

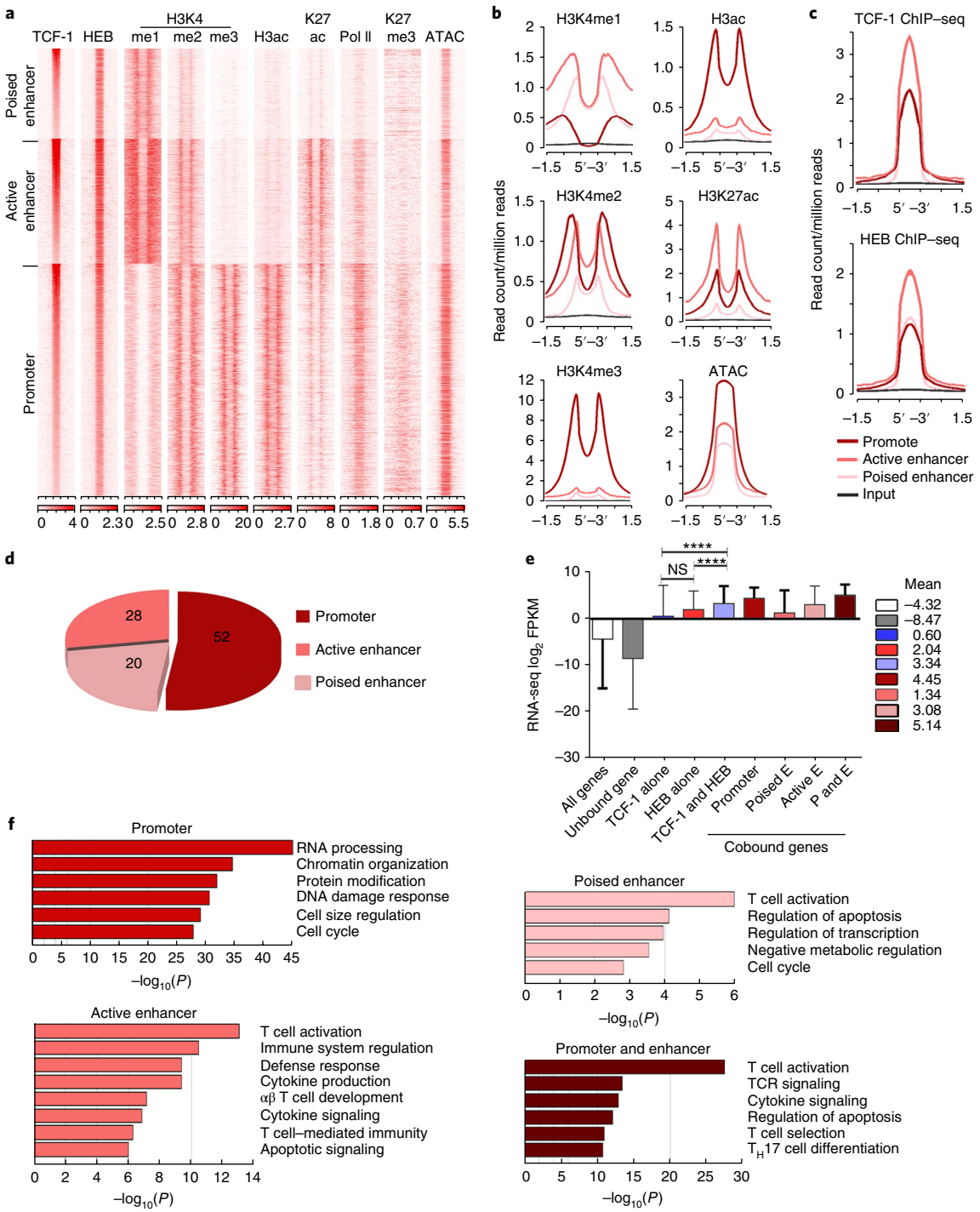

Fig. 4 | TCF-1 and HEB cobind accessible chromatin of highly expressed genes. a, *K*-means-clustered heat map centered on TCF-1 and HEB overlapping sites (±1.5 kb), showing enrichment of the indicated histone modifications and RNA Pol II in WT thymocytes, and ATAC-seq in DP thymocytes (±1.5 kb). **b**, Comparative enrichment histograms of permissive histone modifications (H3ac, H3K4me1, H3K4me2, H3K4me3, and H3K27ac) and chromatin accessibility (ATAC-seq) at overlapping TCF-1- and HEB-binding sites (±1.5 kb) in clusters identified in **a**. **c**, ChIP-seq enrichment of TCF-1 (top) and HEB (bottom) at regions of overlapping TCF-1 and HEB binding identified in **a** (±1.5 kb). **d**, Genomic distribution of overlapping TCF-1- and HEB-binding sites in WT thymocytes. **e**, Average expression in DP thymocytes of genes in the indicated groups. E, enhancer; P, promoter. Numbers are mean $\log_2$ FPKM (****$P \leq 0.0001$, Kruskal–Wallis test; error bars, s.d.). (All genes, $n = 23{,}360$; unbound genes, $n = 13{,}710$; TCF-1 alone, $n = 2{,}630$ genes; HEB alone, $n = 1{,}174$ genes; TCF-1 and HEB, $n = 5{,}846$ genes; promoter, $n = 3{,}098$ genes; active enhancer, $n = 1{,}160$ genes; poised enhancer, $n = 1{,}067$ genes; promoter + enhancer, $n = 521$ genes). **f**, Functional pathways enriched in genes bound by both TCF-1 and HEB in promoters or promoters and enhancers. (Active enhancer, $n = 1{,}160$ genes; poised enhancer, $n = 1{,}067$ genes; promoter, $n = 3{,}098$ genes; promoter + enhancer, $n = 521$ genes). Pathways and statistical enrichment were determined by Metascape.

compared with 12,233 in WT thymocytes, reflecting a 73% decrease (Supplementary Fig. 5a,b). Of these sites, 84% were also bound by HEB in WT thymocytes, and 489 were new. Of the HEB sites in TCF-1-deficient thymocytes (Fig. 5a,b), 68% were cobound by TCF-1 and HEB in WT thymocytes, indicating that HEB binding at these sites does not require the presence of TCF-1. In addition,

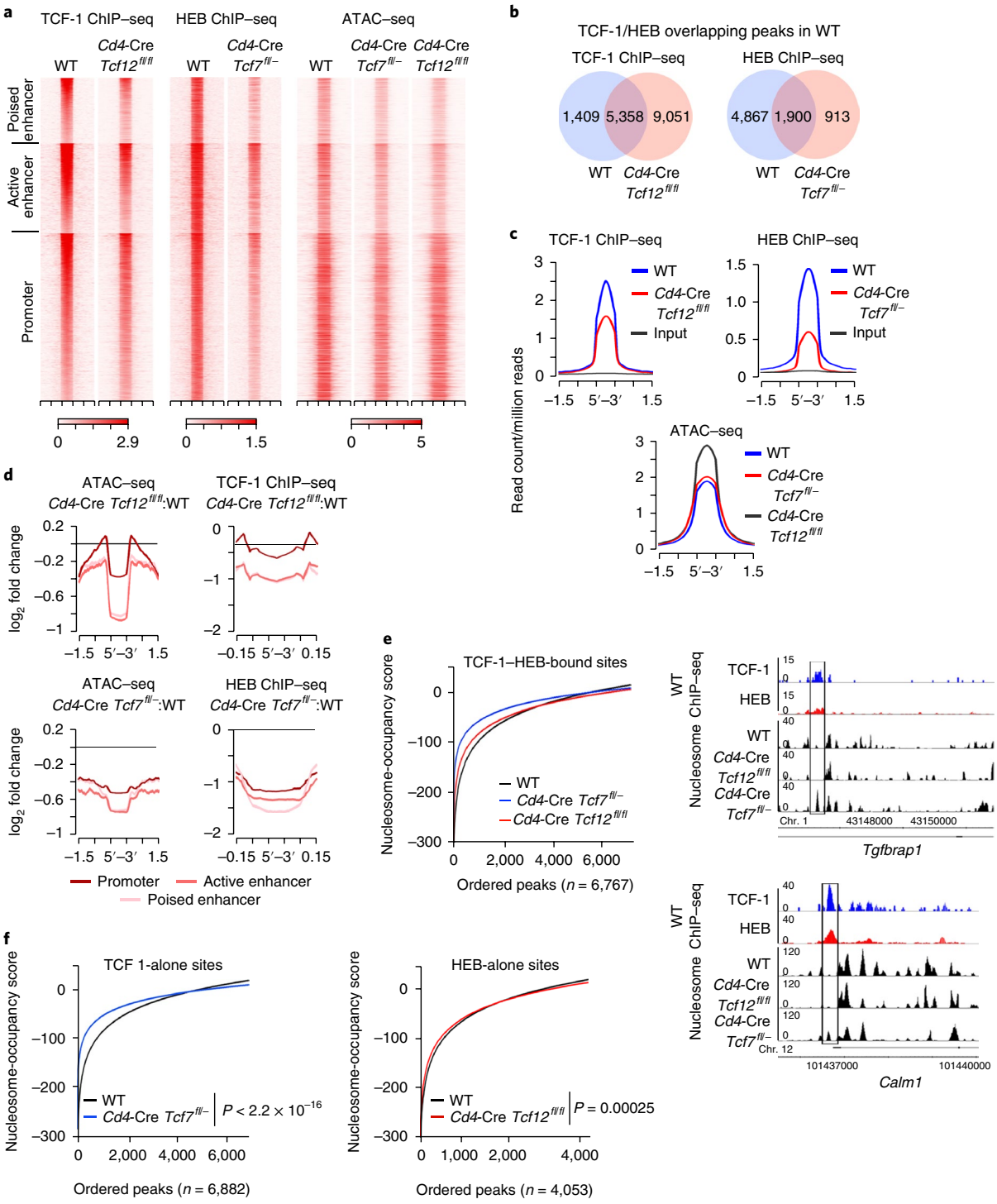

Fig. 5 | TCF-1 and HEB promote chromatin accessibility at cobound sites. a, Heat map of TCF-1 and HEB ChIP–seq enrichment and chromatin accessibility (ATAC–seq) in thymocytes from WT, *Cd4*-Cre *Tcf7*$^{fl/-}$, and *Cd4*-Cre *Tcf12*$^{fl/fl}$ mice (±1.5 kb around overlapping WT TCF-1 and HEB sites). ATAC–seq was performed in sorted DP thymocytes. **b**, Venn diagrams comparing the numbers of TCF-1-bound sites in *Cd4*-Cre *Tcf12*$^{fl/fl}$ thymocytes that overlap with WT TCF-1/HEB-cobound sites (left), and HEB bound sites in *Cd4*-Cre *Tcf7*$^{fl/-}$ thymocytes that overlap with WT TCF-1/HEB-cobound sites (right). **c**, Histogram of TCF-1 enrichment in WT and *Cd4*-Cre *Tcf12*$^{fl/fl}$ thymocytes (top left), HEB enrichment in WT and *Cd4*-Cre *Tcf7*$^{fl/-}$ thymocytes (top right), and chromatin accessibility (bottom, ATAC–seq) in WT, *Cd4*-Cre *Tcf7*$^{fl/-}$, and *Cd4*-Cre *Tcf12*$^{fl/fl}$ DP thymocytes. Plots are centered on overlapping WT TCF-1 and HEB sites (±1.5 kb). **d**, Histograms of $\log_2$ fold change in accessibility (ATAC–seq) and transcription-factor enrichment in the indicated mutants compared with WT thymocytes, at genomic regions centered on TCF-1 and HEB overlapping sites in WT thymocytes (±1.5 kb). **e**, Nucleosome-occupancy scores at TCF-1 and HEB overlapping sites in WT thymocytes. Negative values indicate nucleosome absence, and positive values indicate nucleosome presence (WT = –50.1028; *Cd4*-Cre *Tcf12*$^{fl/fl}$ = –46.2251; *Cd4*-Cre *Tcf7*$^{fl/-}$ = –30.5216). Representative tracks of nucleosome appearance in the absence of TCF-1 within TCF-1 and HEB overlapping sites at the *Tgfbrap1* and *Calm1* loci. **f**, Left, nucleosome-occupancy scores in WT and *CD4*-Cre/*Tcf1*$^{fl/-}$ DP thymocytes at WT TCF-1-binding sites without HEB. Right, nucleosome-occupancy scores in WT and *Cd4*-Cre *Tcf12*$^{fl/fl}$ DP thymocytes at WT HEB-binding sites without TCF-1. *P* values were determined by the Mann–Whitney–Wilcoxon test.

the average enrichment of HEB at the remaining binding sites was also markedly lower in TCF-1-deficient than WT thymocytes (Fig. 5c and Supplementary Fig. 5c). HEB enrichment was most decreased at poised enhancers, followed by active enhancers and then promoters (Fig. 5d). The number of TCF-1-binding sites was only moderately lower in HEB-deficient than HEB-containing thymocytes (from 16,377 to 14,409). Of these remaining sites, 10,007 (70%) overlapped with TCF-1-binding sites in WT thymocytes, whereas 4,402 were new (Supplementary Fig. 5d,e). Although most TCF-1-bound sites were maintained in the absence of HEB, TCF-1 enrichment in the remaining sites was decreased (Fig. 5c and Supplementary Fig. 5f). Similarly to HEB binding, TCF-1 binding was also primarily decreased at active and poised enhancers (Fig. 5d). Thus, TCF-1 and HEB each affect the enrichment of the other on DNA; however, the severe decrease in the number of HEB-binding sites in TCF-1-deficient cells is likely to be an indirect effect of the absence of TCF-1.

TCF-1 has multiple epigenetic and chromatin conformation functions[18,21]; however, a role for HEB in shaping the chromatin has not yet been established[23]. Therefore, we examined the effect of TCF-1 and HEB on the chromatin landscape. We compared chromatin accessibility in WT and TCF-1- or HEB-deficient DP thymocytes by using ATAC–seq (Supplementary Fig. 6). We found 51,452 ($P=1.0\times10^{-5}$) accessible regions in WT cells, and fewer in TCF-1-deficient (48,479 sites) or HEB-deficient (42,237 sites) DP thymocytes. In WT accessible regions, two of the top five enriched motifs were TCF-1 ($P=1\times10^{-198}$) and HEB ($P=1\times10^{-274}$) motifs (Supplementary Fig. 6a). TCF-1 ($P=1\times10^{-82}$) and HEB ($P=1\times10^{-112}$) were also among the five most enriched motifs in the 7,241 sites that were accessible in WT but lost accessibility after ablation of TCF-1 or HEB (Supplementary Fig. 6e). However, accessible regions in TCF-1-deficient and HEB-deficient DP thymocytes were relatively depleted in TCF-1 and HEB conserved motifs, as compared with WT (Supplementary Fig. 6b,c). Importantly, regions that gained accessibility in TCF-1- or HEB-deficient DP thymocytes were not enriched in TCF-1 or HEB motifs (Supplementary Fig. 6f,g). Additionally, novel HEB- and TCF-1-binding sites detected in TCF-1- or HEB-deficient thymocytes, respectively, were not at these newly accessible regions. These findings demonstrate that TCF-1 and HEB promote accessibility at sites containing TCF-1 and HEB motifs. Moreover, they indicate that E2A, the partner of HEB, does not significantly compensate for the loss of accessibility at HEB-motif-containing sites.

Genomic sites bound by TCF-1 or HEB in WT thymocytes were less accessible in HEB- or TCF-1-deficient DP thymocytes, respectively, and binding enrichment was greatly decreased (Supplementary Fig. 5c,f). Importantly, TCF-1/HEB-cobound sites were also less accessible in the absence of either TCF-1 or HEB (Fig. 5a,c). The degree of accessibility loss was more pronounced at cobound enhancers, particularly active enhancers (Fig. 5d), where the TCF-1 and HEB binding enrichment was highest (Fig. 4c). The novel finding that HEB deletion decreased chromatin accessibility is consistent with its known interaction with p300 (ref. [23]) and establishes that HEB has genome-wide epigenetic functions.

We next examined whether decreased chromatin accessibility in the absence of TCF-1 or HEB might also reflect changes in the nucleosome landscape. Nucleosome tracks were generated from paired-end ATAC–seq of WT, TCF-1-deficient, and HEB-deficient DP thymocytes. The nucleosome occupancy at TCF-1/HEB-cobound sites was calculated with the UCSC tool bigWigAverageOverBed. This tool assigns a probability score for the presence of a nucleosome at each site. Positive values indicate high probability, and negative values indicate low probability. In agreement with the decreased chromatin accessibility, the probability that nucleosomes occupied TCF-1/HEB-cobound sites was higher in TCF-1- and HEB-deficient DP thymocytes than WT thymocytes (Fig. 5e). However, although the probability of nucleosome occupancy was substantially higher in TCF-1-deficient DP thymocytes ($P<2.2\times10^{-16}$), the increase in HEB-deficient DP thymocytes was only marginally significant ($P=0.0012$; Fig. 5e). De novo nucleosome occupancy at TCF-1/HEB-cobound sites in TCF-1-deficient thymocytes is also shown for the *Tgfbrap1* and *Calm1* genes. This finding is in line with a recent report demonstrating that TCF-1 can shift nucleosomes[21]. The dominant role of TCF-1 in controlling nucleosome occupancy was further confirmed for sites uniquely bound by TCF-1 or by HEB in WT thymocytes (Fig. 5f). The nucleosome occupancy at sites bound by TCF-1 alone was substantially higher in TCF-1-deficient DP thymocytes ($P<2.2\times10^{-16}$). However, at sites bound by HEB alone, this increase in HEB-deficient thymocytes was only marginally significant ($P=0.00025$). Overall, our findings show that TCF-1 and HEB coordinately regulate chromatin accessibility, and TCF-1 has a dominant role in controlling the presence of nucleosomes at cobound sites in DP thymocytes.

TCF-1/HEB cobinding to their motifs promotes gene expression. Several DP-thymocyte processes depend on the presence of TCF-1 and HEB. Therefore, we investigated whether the TCF-1/HEB cobinding in DP thymocytes might reflect regulation of overlapping transcriptional programs. We identified significant ($P=0.05$) gene expression changes in both TCF-1-deficient ($n=1,269$) and HEB-deficient ($n=838$) DP thymocytes compared with WT thymocytes. Spearman's rank-correlation comparison of the two sets established that transcriptional changes associated with TCF-1 deficiency mirrored the transcriptional changes associated with HEB deficiency (Spearman correlation = 0.36, $P=1.99\times10^{-61}$; Fig. 6a). This finding establishes that through their extensive cobinding and epigenetic functions, TCF-1 and HEB cooperatively regulate the transcriptional profile of DP thymocytes.

Ablation of either TCF-1 or HEB limited binding of the other factor to DNA and decreased chromatin accessibility, particularly at active enhancers. To determine whether TCF-1/HEB cobinding at distinct regulatory regions differentially modulates gene transcription, we compared expression changes in WT versus TCF-1- or HEB-deficient DP thymocytes, according to the region bound. TCF-1/HEB-cobound genes in WT thymocytes were divided into clusters exhibiting promoter-only binding, enhancer-only binding (poised or active), or both promoter and enhancer binding (poised or active). Expression changes in WT versus TCF-1-deficient and WT versus HEB-deficient DP thymocytes within these clusters were subjected to cumulative distribution function (CDF) analysis and compared to expression changes of all genes (Fig. 6b). TCF-1/HEB cobinding at promoter-only or poised enhancer-only clusters was equally likely to confer up- or downregulation of the associated gene. Notably, TCF-1/HEB cobinding at active enhancer sites or both enhancer and promoter sites was significantly more likely to promote upregulation of the associated gene. Thus, DNA binding and epigenetic and transcriptional analyses cumulatively established that TCF-1/HEB cobinding to active enhancers or enhancers and promoters increases chromatin accessibility and promotes expression of the associated genes.

We found that TCF-1 and HEB promote accessibility at sites containing TCF-1 and HEB motifs (Supplementary Fig. 6). However, not all TCF-1/HEB-cobound sites contain TCF-1 and HEB motifs. Therefore we tested whether the transcription of gene targets was dependent on TCF-1 and HEB binding to their motifs. Cobound regions were subdivided into two clusters on the basis of whether they contained TCF-1 and HEB motifs. The expression changes of genes associated with each cluster in WT versus TCF-1-deficient and WT versus HEB-deficient thymocytes were compared with the expression changes of all genes in CDF analyses (Fig. 6c). Genes associated with motifs containing TCF-1 and HEB peaks were significantly more likely to be downregulated under ablation of either

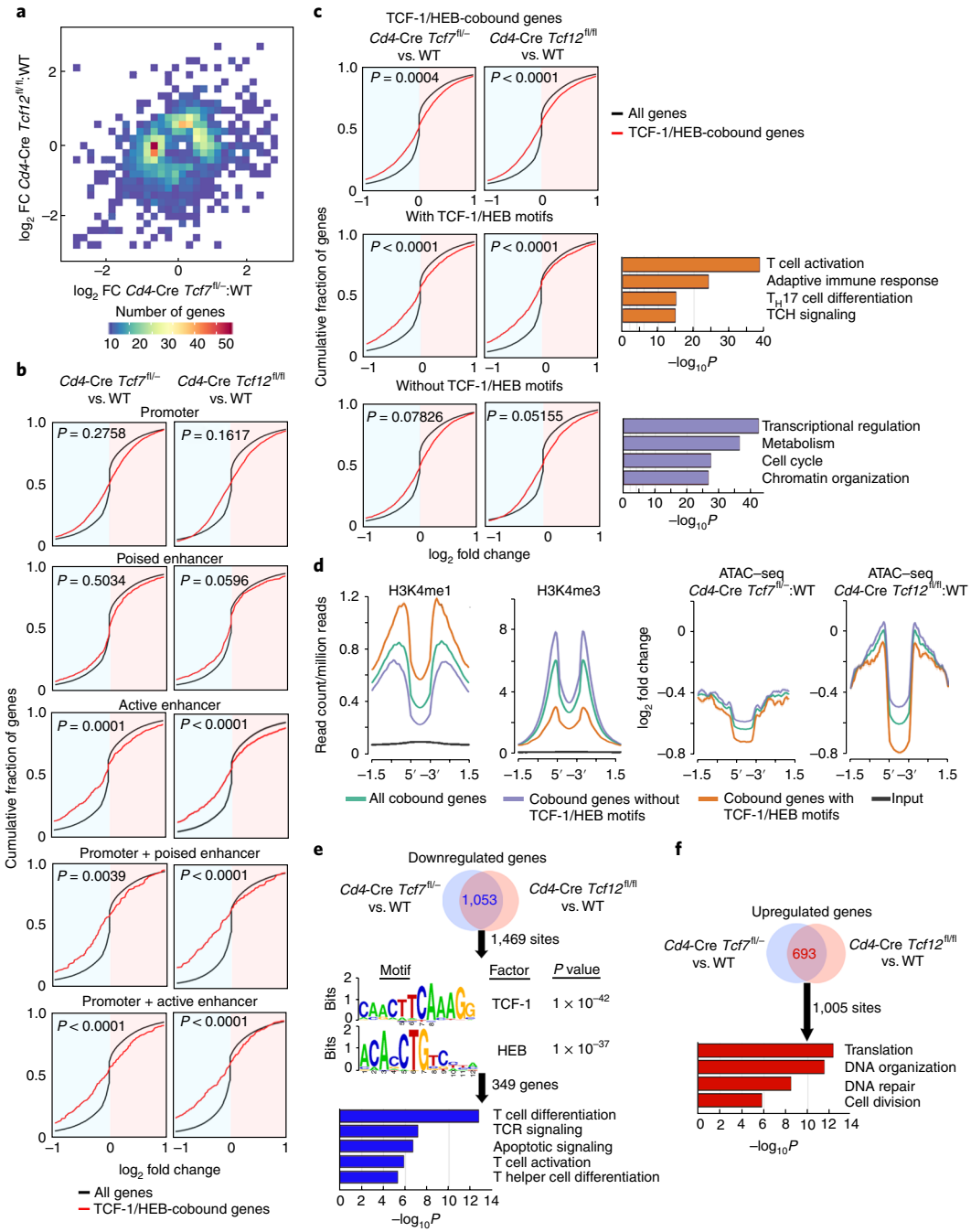

Fig. 6 | TCF-1 and HEB cooperatively influence DP-thymocyte gene expression. a, Spearman's correlation analysis performed on genes whose expression significantly changed ($n = 1{,}834$, $P \leq 0.05$, Cuffdiff) between WT versus *Cd4*-Cre *Tcf12*$^{fl/fl}$ DP thymocytes (*y* axis), and WT versus *Cd4*-Cre *Tcf7*$^{fl/-}$ DP thymocytes (*x* axis). Positive Spearman's correlation, 0.36, indicates similar changes. FC, fold change. **b**, CDF plot of expression changes in *Cd4*-Cre *Tcf7*$^{fl/-}$ versus WT (left) or *Cd4*-Cre *Tcf12*$^{fl/fl}$ versus WT (right) for genes bound by TCF-1 and HEB in WT thymocytes. Black curves indicate expression changes of all genes expressed in DP thymocytes, and red curves indicate expression changes of genes bound by TCF-1 and HEB in the indicated genomic regions. $\log_2$ expression changes are shown; *P* values indicate the significance of the difference between red and black curves (two-tailed Mann–Whitney *U* test). (Promoter, 2,577 genes; poised enhancer, 661 genes; active enhancer, 624 genes; promoter + poised enhancer, 154 genes; promoter + active enhancer, 283 genes; all black curves, 23,360 genes. **c**, CDF plot of expression changes as in **b** of all genes bound by TCF-1 and HEB in WT (top) thymocytes, genes bound by TCF-1 and HEB at sites that contain their conserved motifs (middle), and genes bound by TCF-1 and HEB at sites that do not contain their conserved motifs (bottom). Pathways enriched within genes containing or lacking motifs are shown next to the relevant CDF plot. *P* values were determined with a two-tailed Mann–Whitney *U* test. (All cobound genes, $n = 4{,}299$; genes with TCF-1 and HEB motifs, $n = 1{,}790$; genes without TCF-1 and HEB motifs, $n = 2{,}509$. **d**, Comparative enrichment histogram plots of the indicated histone marks and changes in chromatin accessibility centered on TCF-1 and HEB binding sites (±1.5 kb) at the indicated sites. **e**, Number of overlapping downregulated genes ($P \leq 0.05$, Cuffdiff) (top) in TCF-1- or HEB-deficient DP thymocytes (RNA-seq) within 20 kb of TCF-1/HEB-cobound sites identified with BETA. Middle, enriched motifs in the TCF-1/HEB-cobound sites (1,469) within 20 kb of downregulated genes. Bottom, Metascape pathways enriched within downregulated genes with TCF-1 and HEB motifs identified by BETA (349 genes). **f**, Number of overlapping upregulated genes ($P \leq 0.05$, Cuffdiff) (top) identified by BETA (693) within 20 kb of TCF-1/HEB-cobound sites (1,005 sites). Bottom, Metascape pathways enriched in upregulated genes.

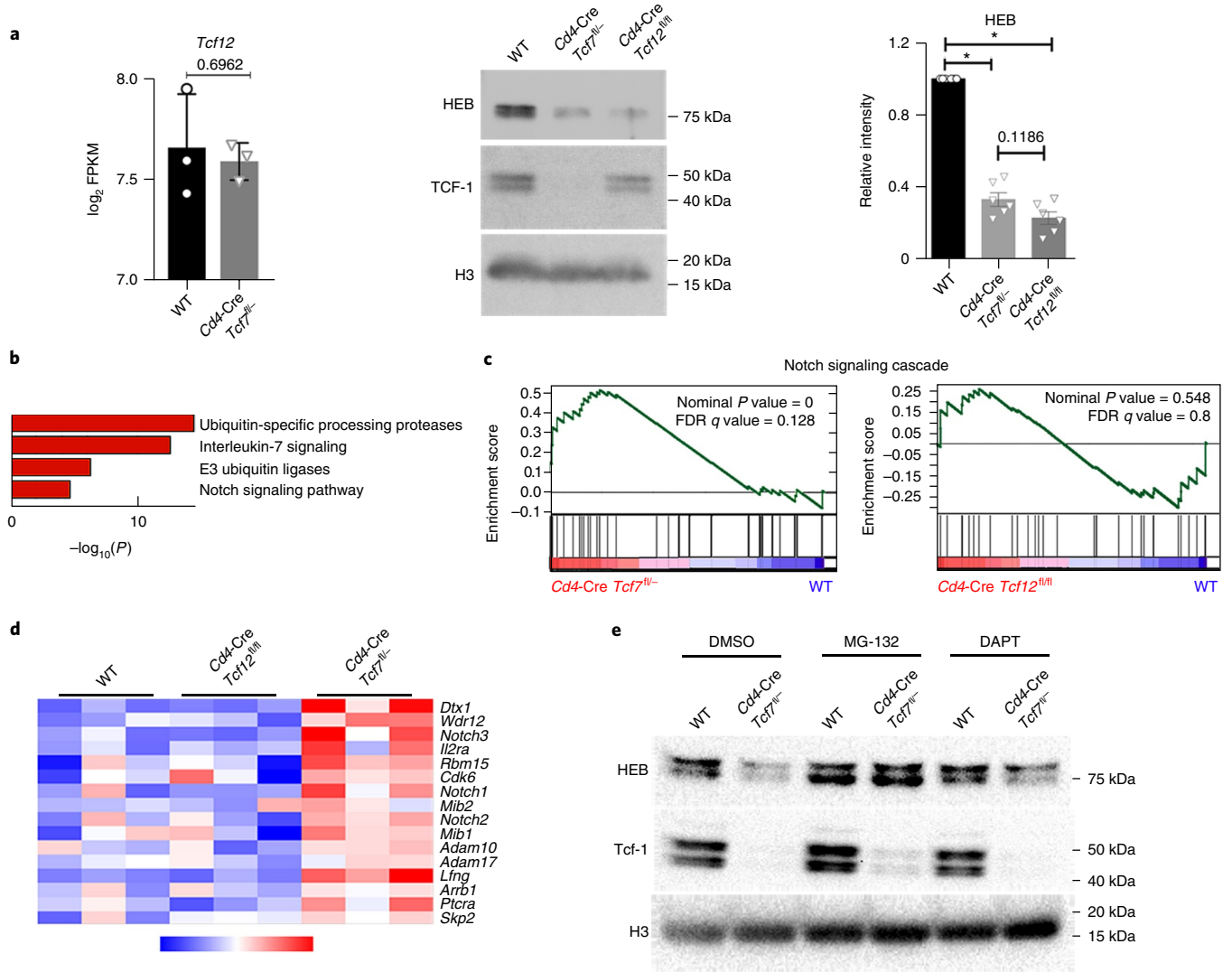

Fig. 7 | TCF-1 promotes HEB stability by inhibiting Notch signaling. a, Left, $\log_2$ FPKM of HEB transcripts in RNA-seq from sorted WT and TCF-1-deficient DP thymocytes ($n = 3$ biologically independent samples; WT mean, 7.61; *Cd4*-Cre *Tcf7*$^{fl/-}$ mean, 7.52). *P* value was determined with a two-tailed unpaired *t* test; error bars, s.d. Middle, immunoblot analysis of HEB and TCF-1 protein expression in WT, *Cd4*-Cre *Tcf7*$^{fl/-}$, and *Cd4*-Cre *Tcf12*$^{fl/fl}$ sorted DP thymocytes. H3, loading control. Right, HEB protein quantification (Image Lab) in flow cytometry–sorted WT, *Cd4*-Cre *Tcf7*$^{fl/-}$, and *Cd4*-Cre *Tcf12*$^{fl/fl}$ DP thymocytes, normalized to WT quantities *P* values were determined with a two-tailed Wilcoxon signed-rank test ($n = 6$ biologically independent samples). **b**, Metascape pathway enrichment of genes only upregulated in *Cd4*-Cre *Tcf7*$^{fl/-}$ DP thymocytes compared with WT DP thymocytes. **c**, Gene-set enrichment analysis of the Notch signaling cascade (Hallmark_Notch_signaling) in TCF-1-deficient and HEB-deficient DP thymocytes. On the *x* axis, genes are ranked from most upregulated (left) to most downregulated (right) between mutant and WT DP thymocytes. The *y* axis indicates the enrichment scores of genes in the pathway. **d**, Heat map of the expression (RNA-seq) of genes in the Notch signaling cascade ($n = 3$ biologically distinct samples of WT, *Cd4*-Cre *Tcf12*$^{fl/fl}$, and *Cd4*-Cre *Tcf7*$^{fl/-}$ DP thymocytes). **e**, Immunoblot analysis of HEB and TCF-1 protein levels in sorted DP thymocytes from WT and *Cd4*-Cre *Tcf7*$^{fl/-}$ mice cultured with DMSO vehicle control, MG132 (5 μm), or DAPT (10 μm) for 6 h. H3, loading control. Results are representative of 3 independent experiments.

TCF-1 or HEB and were enriched in T cell–development pathways (Supplementary Table 1). However, genes associated with TCF-1 and HEB peaks lacking TCF-1 and HEB motifs did not show consistent changes and were enriched in cell-cycle and chromatin processes (Supplementary Table 2). Our two independent CDF analyses showed that TCF-1/HEB cobinding to active enhancers or to their conserved motifs promoted gene expression. To link these findings, we assessed the genomic location of cobound regions containing TCF-1 and HEB motifs to regions lacking such motifs, on the basis of their chromatin landscape. Sites containing TCF-1 and HEB motifs were highly enriched in the enhancer H3K4me1 mark, whereas sites lacking these motifs were more enriched in the promoter mark H3K4me3 (Fig. 6d). Thus, TCF-1/HEB cobinding to sites that contain their conserved motif predominantly at enhancers promotes expression of the corresponding genes.

To independently establish that TCF-1/HEB cobinding to their conserved motifs correlates with gene upregulation, we performed binding and expression target analysis (BETA)[41]. Using BETA, we identified in WT shared TCF-1 and HEB peaks located within 20 kb of the transcription start sites of genes that changed in expression in the absence of TCF-1 or HEB compared with WT. The 1,053 genes commonly downregulated in the absence of TCF-1 or HEB represented 1,469 TCF-1/HEB-cobound sites (Fig. 6e). Additionally, the 693 commonly upregulated genes represented 1,005 TCF-1/HEB-cobound sites (Fig. 6f). In agreement with the CDF analyses, motif enrichment at these shared sites differentiated downregulated from

upregulated genes. Only downregulated genes showed enrichment in TCF-1 ($P=1\times10^{-42}$) and HEB ($P=1\times10^{-37}$) motifs (Fig. 6e). Analysis of motif-containing sites identified 349 genes involved in T cell–differentiation processes (Fig. 6e). In contrast, the 693 upregulated genes that lacked TCF-1- and HEB-motif enrichment were involved in proliferation and DNA-repair processes. Overall, our analyses indicate that cobinding of TCF-1 and HEB to their conserved motifs, predominantly at enhancers, promotes the expression of genes essential for DP thymocyte development.

TCF-1 regulates HEB stability by limiting Notch signaling. We showed that TCF-1 and HEB coordinately regulate the chromatin landscape and transcription profiles of DP thymocytes. However, it was unclear why HEB binding was severely decreased in TCF-1-deficient thymocytes, whereas TCF-1 binding was less affected in HEB-deficient thymocytes. *Tcf12* mRNA abundance was similar between WT and TCF-1-deficient cells (Fig. 7a). However, immunoblot analyses showed that HEB protein expression was potently decreased and comparable to that observed in HEB-deficient DP thymocytes (Fig. 7a). Notch signaling was previously reported to induce ubiquitination of E2A, thus resulting in its degradation[42–44]. We investigated whether a similar process might have decreased HEB protein abundance in TCF-1-deficient DP thymocytes. Our RNA-seq data showed that the Notch and ubiquitination pathways were transcriptionally upregulated in TCF-1-deficient DP thymocytes (Fig. 7b). Gene-set enrichment analysis showed that the Notch signaling cascade (Hallmark_Notch_signaling) was selectively upregulated in TCF-1-deficient but not HEB-deficient DP thymocytes compared with WT thymocytes (Fig. 7c,d). In particular, TCF-1 bound without HEB to 103 regions of Notch-pathway genes (Supplementary Fig. 7). Two-thirds of these regions were at enhancers, and histone-mark enrichment as well as accessibility patterns most closely corresponded to poised enhancers. However, TCF-1 ablation did not decrease accessibility at these sites as severely as at TCF-1/HEB- cobound poised/active enhancers, thus potentially allowing for transcription of the corresponding Notch-pathway genes.

To determine whether the upregulation of the Notch and ubiquitin ligase pathways caused the decreased HEB protein abundance in TCF-1-deficient thymocytes, we sorted WT and TCF-1-deficient DP thymocytes and performed immunoblot analysis to assess HEB protein after treatment with the proteasome inhibitor MG132 (5 μM) or the Notch inhibitor DAPT (10 μM). Both proteasome and Notch inhibition restored HEB protein abundance in TCF-1-deficient DP thymocytes (Fig. 7e). These findings indicate that ablation of TCF-1 increases Notch signaling and consequently promotes proteasomal degradation of HEB. Therefore, by inhibiting Notch signaling, TCF-1 stabilizes HEB, thus allowing for their coordinated functions at the DP stage of thymocyte development.

Discussion

Thymocytes transitioning to the DP stage cease proliferating, rearrange the *Tcra* gene, and assemble the αβ TCR[45]. Coordinating these events requires precise transcriptional and epigenetic reprograming of developing thymocytes. Here, we identified TCF-1 and HEB as cooperating partners regulating chromatin accessibility and gene expression in DP thymocytes, We show that TCF-1 and HEB cooperatively halt the proliferation of early DP thymocytes and promote survival and T cell development. This regulation involves extensive overlap of TCF-1 and HEB DNA binding. TCF-1 and HEB promote chromatin accessibility, whereas predominantly TCF-1 minimizes nucleosome occupancy. Importantly, TCF-1 stabilizes HEB protein by limiting its Notch-mediated proteasomal degradation.

Developmental programs depend on the coordination of regulators and epigenetic organizers[3,4,7,8,10,46,47]. Here, we found that TCF-1, which reaches its highest expression in DP thymocytes (https://www.immgen.org/), binds the promoters and enhancers of highly expressed genes, where it shares binding sites with other factors, including Runx1, Ikaros, and HEB. The essential functions of TCF-1 (refs [4,14,15,39]), HEB[16,29,48,49], Runx1 (ref. [34]), and Ikaros[50] in thymocyte development, and their differential abilities to modulate chromatin landscapes, suggest that they regulate this developmental process through a complex interplay. In early thymic development, TCF-1 has been shown to coordinate with Notch1, GATA-3, and Runx1, in a proccess that culminates in Bcl11b activation and T cell commitment[7]. Furthermore, a recent report has demonstrated that TCF-1 promotes de novo chromatin opening[21].

Our study focused on the cooperation between TCF-1 and HEB at the DP stage, in which the two factors share an extensive number of binding sites as well as common developmental functions. Particularly, ablation of either TCF-1 or HEB decreases DP-thymocyte survival, affects development of natural killer T cells[26,27], and increases DP-thymocyte proliferation. TCF-1 and HEB share binding to sites that contain their conserved motifs predominantly at the enhancers of genes involved in T cell development and positively co-regulate their expression. In contrast, TCF-1 and HEB share binding sites lacking their conserved motifs and negatively co-regulate the expression of genes involved in proliferation.

Although HEB binds the histone acetyltransferase p300 (ref. [23]), it has not been directly shown to modulate the chromatin landscape. Here, we demonstrate that HEB promotes chromatin accessibility genome wide in DP thymocytes. This epigenetic function of HEB is distinct from the epigenetic functions of TCF-1, because HEB-deficient cells have diminished chromatin accessibility despite normal TCF-1 protein abundance. Additionally, the accessibility-promoting functions of HEB and TCF-1 are not complementary. Chromatin closing in HEB-deficient cells, which maintain TCF-1 protein, is comparable to that in TCF-1-deficient cells, which also lose HEB protein expression. Moreover, E2A, the interacting partner of HEB[22,29], does not compensate for the epigenetic functions of HEB, because HEB-deficient DP thymocytes specifically lose accessibility in regions containing the common HEB/E2A-binding motif. In agreement with promoting chromatin accessibility, predominantly TCF-1, and marginally HEB, limit nucleosome occupancy in their cobound sites. This conclusion is supported by the finding that sites uniquely bound by TCF-1 have increased nucleosome presence, whereas sites uniquely bound by HEB show only a marginal increase after loss of TCF-1 or HEB, respectively. Altogether, our findings suggest that TCF-1 and HEB coordinately shape the chromatin landscape of DP thymocytes; both are needed for promoting chromatin accessibility, but they do not have complementary effects. In contrast, TCF-1 has a dominant role over HEB in regulating the nucleosomal landscape.

We discovered that, beyond TCF-1 and HEB binding the same genomic locations and mediating epigenetic and transcriptional regulation, TCF-1 regulates HEB protein stability. TCF-1 accomplishes this function through a higher-level coordination whereby TCF-1 controls the levels of Notch signaling, and Notch signaling in turn controls HEB stability. The targeting of HEB by Notch signaling parallels the previously established Notch-mediated targeting of E2A, a possible heterodimerization partner of HEB, for ubiquitination and proteasomal degradation[42–44]. Notch signaling is gradually downregulated as cells progress to the DP stage, whereas the activity of TCF-1 and HEB is essential for the transition into the DP stage. Our data suggest that TCF-1 mediates the downregulation of Notch, thereby facilitating stabilization of the HEB protein, which in turn enables their coordinated actions in promoting DP-thymocyte development.

Our studies offer a novel understanding of the complex regulatory network that controls DP-thymocyte development. We demonstrate that TCF-1/HEB cobinding to promoters versus enhancers, identifies genes involved in distinct processes and differentially

affects their transcription and epigenetic status. TCF-1 has an epistatic role in regulating common TCF-1 and HEB functions through its ability to stabilize the HEB protein by modulating Notch signaling. TCF-1/HEB-cobound sites are enriched for different transcription-factor motifs. Cobound genes that are downregulated by the presence of TCF-1 and HEB lack the conserved TCF-1 and HEB motifs. This result suggests that TCF-1 and HEB potentially organize and/or participate in complex networks of regulators that change dynamically as cells enter and progress within the DP stage. Future studies are expected to decipher the complex orchestration between TCF-1 and Notch signaling in the regulation of HEB. Additionally, future studies will address the coordination of TCF-1 and HEB with other lymphoid factors, such as Runx1 and Ikaros, and their combined effects on chromatin organization, gene expression, and DP-thymocyte development.

Online content

Any methods, additional references, Nature Research reporting summaries, source data, statements of data availability and associated accession codes are available at https://doi.org/10.1038/s41590-018-0254-4.

Received: 28 April 2018; Accepted: 11 October 2018;
Published online: 12 November 2018

References

1. Klein, L., Kyewski, B., Allen, P. M. & Hogquist, K. A. Positive and negative selection of the T cell repertoire: what thymocytes see (and don't see). *Nat. Rev. Immunol.* **14**, 377–391 (2014).
2. Maillard, I., Fang, T. & Pear, W. S. Regulation of lymphoid development, differentiation, and function by the Notch pathway. *Annu. Rev. Immunol.* **23**, 945–974 (2005).
3. Weber, B. N. et al. A critical role for TCF-1 in T-lineage specification and differentiation. *Nature* **476**, 63–68 (2011).
4. Germar, K. et al. T-cell factor 1 is a gatekeeper for T-cell specification in response to Notch signaling. *Proc. Natl Acad. Sci. USA* **108**, 20060–20065 (2011).
5. García-Ojeda, M. E. et al. GATA-3 promotes T-cell specification by repressing B-cell potential in pro-T cells in mice. *Blood* **121**, 1749–1759 (2013).
6. Scripture-Adams, D. D. et al. GATA-3 dose-dependent checkpoints in early T cell commitment. *J. Immunol.* **193**, 3470–3491 (2014).
7. Kueh, H. Y. et al. Asynchronous combinatorial action of four regulatory factors activates Bcl11b for T cell commitment. *Nat. Immunol.* **17**, 956–965 (2016).
8. Kumata, K. et al. Development of [^{11}C]MFTC for PET imaging of fatty acid amide hydrolase in rat and monkey brains. *ACS Chem. Neurosci.* **6**, 339–346 (2015).
9. Hosokawa, H. et al. Transcription factor PU.1 represses and activates gene expression in early T cells by redirecting partner transcription factor binding. *Immunity* **48**, 1119–1134.e1117 (2018).
10. Longabaugh, W. J. R. et al. Bcl11b and combinatorial resolution of cell fate in the T-cell gene regulatory network. *Proc. Natl Acad. Sci. USA* **114**, 5800–5807 (2017).
11. Wang, D. et al. The basic helix-loop-helix transcription factor HEBAlt is expressed in pro-T cells and enhances the generation of T cell precursors. *J. Immunol.* **177**, 109–119 (2006).
12. Yücel, R., Kosan, C., Heyd, F. & Möröy, T. Gfi1:green fluorescent protein knock-in mutant reveals differential expression and autoregulation of the growth factor independence 1 (Gfi1) gene during lymphocyte development. *J. Biol. Chem.* **279**, 40906–40917 (2004).
13. David-Fung, E. S. et al. Transcription factor expression dynamics of early T-lymphocyte specification and commitment. *Dev. Biol.* **325**, 444–467 (2009).
14. Verbeek, S. et al. An HMG-box-containing T-cell factor required for thymocyte differentiation. *Nature* **374**, 70–74 (1995).
15. Schilham, M. W. et al. Critical involvement of Tcf-1 in expansion of thymocytes. *J. Immunol.* **161**, 3984–3991 (1998).
16. Barndt, R., Dai, M. F. & Zhuang, Y. A novel role for HEB downstream or parallel to the pre-TCR signaling pathway during alpha beta thymopoiesis. *J. Immunol.* **163**, 3331–3343 (1999).
17. Clevers, H. Wnt/beta-catenin signaling in development and disease. *Cell* **127**, 469–480 (2006).
18. Mosimann, C., Hausmann, G. & Basler, K. Beta-catenin hits chromatin: regulation of Wnt target gene activation. *Nat. Rev. Mol. Cell Biol.* **10**, 276–286 (2009).
19. Clevers, H. & Nusse, R. Wnt/β-catenin signaling and disease. *Cell* **149**, 1192–1205 (2012).
20. Xing, S. et al. Tcf1 and Lef1 transcription factors establish CD8$^+$ T cell identity through intrinsic HDAC activity. *Nat. Immunol.* **17**, 695–703 (2016).
21. Johnson, J. L. et al. Lineage-determining transcription factor TCF-1 initiates the epigenetic identity of T cells. *Immunity* **48**, 243–257.e210 (2018).
22. Kee, B. L. E and ID proteins branch out. *Nat. Rev. Immunol.* **9**, 175–184 (2009).
23. Williams, C. J. et al. The chromatin remodeler Mi-2beta is required for CD4 expression and T cell development. *Immunity* **20**, 719–733 (2004).
24. Huang, Z. et al. Transcriptional regulation of CD4 gene expression by T cell factor-1/beta-catenin pathway. *J. Immunol.* **176**, 4880–4887 (2006).
25. Ioannidis, V., Beermann, F., Clevers, H. & Held, W. The β-catenin–TCF-1 pathway ensures CD4$^+$CD8$^+$ thymocyte survival. *Nat. Immunol.* **2**, 691–697 (2001).
26. Sharma, A., Berga-Bolaños, R. & Sen, J. M. T cell factor-1 controls the lifetime of CD4$^+$ CD8$^+$ thymocytes in vivo and distal T cell receptor α-chain rearrangement required for NKT cell development. *PLoS One* **9**, e115803 (2014).
27. D'Cruz, L. M., Knell, J., Fujimoto, J. K. & Goldrath, A. W. An essential role for the transcription factor HEB in thymocyte survival, Tcra rearrangement and the development of natural killer T cells. *Nat. Immunol.* **11**, 240–249 (2010).
28. Steinke, F. C. et al. TCF-1 and LEF-1 act upstream of Th-POK to promote the CD4$^+$ T cell fate and interact with Runx3 to silence CD4 in CD8$^+$ T cells. *Nat. Immunol.* **15**, 646–656 (2014).
29. Jones-Mason, M. E. et al. E protein transcription factors are required for the development of CD4$^+$ lineage T cells. *Immunity* **36**, 348–361 (2012).
30. Dose, M. et al. β-catenin induces T-cell transformation by promoting genomic instability. *Proc. Natl Acad. Sci. USA* **111**, 391–396 (2014).
31. Li, L. et al. A far downstream enhancer for murine Bcl11b controls its T-cell specific expression. *Blood* **122**, 902–911 (2013).
32. Winandy, S., Wu, P. & Georgopoulos, K. A dominant mutation in the Ikaros gene leads to rapid development of leukemia and lymphoma. *Cell* **83**, 289–299 (1995).
33. Tinsley, K. W. et al. Ikaros is required to survive positive selection and to maintain clonal diversity during T-cell development in the thymus. *Blood* **122**, 2358–2368 (2013).
34. Egawa, T., Tillman, R. E., Naoe, Y., Taniuchi, I. & Littman, D. R. The role of the Runx transcription factors in thymocyte differentiation and in homeostasis of naive T cells. *J. Exp. Med.* **204**, 1945–1957 (2007).
35. Zhang, J. et al. Harnessing of the nucleosome-remodeling-deacetylase complex controls lymphocyte development and prevents leukemogenesis. *Nat. Immunol.* **13**, 86–94 (2011).
36. Yu, M. et al. Direct recruitment of polycomb repressive complex 1 to chromatin by core binding transcription factors. *Mol. Cell* **45**, 330–343 (2012).
37. Okamura, R. M. et al. Redundant regulation of T cell differentiation and TCRalpha gene expression by the transcription factors LEF-1 and TCF-1. *Immunity* **8**, 11–20 (1998).
38. Held, W., Clevers, H. & Grosschedl, R. Redundant functions of TCF-1 and LEF-1 during T and NK cell development, but unique role of TCF-1 for Ly49 NK cell receptor acquisition. *Eur. J. Immunol.* **33**, 1393–1398 (2003).
39. Yu, S. et al. The TCF-1 and LEF-1 transcription factors have cooperative and opposing roles in T cell development and malignancy. *Immunity* **37**, 813–826 (2012).
40. Whyte, W. A. et al. Master transcription factors and mediator establish super-enhancers at key cell identity genes. *Cell* **153**, 307–319 (2013).
41. Wang, S. et al. Target analysis by integration of transcriptome and ChIP-seq data with BETA. *Nat. Protoc.* **8**, 2502–2515 (2013).
42. Nie, L., Xu, M., Vladimirova, A. & Sun, X. H. Notch-induced E2A ubiquitination and degradation are controlled by MAP kinase activities. *EMBO J.* **22**, 5780–5792 (2003).
43. Nie, L. et al. Notch-induced Asb2 expression promotes protein ubiquitination by forming non-canonical E3 ligase complexes. *Cell Res.* **21**, 754–769 (2011).
44. Li, X., Gounari, F., Protopopov, A., Khazaie, K. & von Boehmer, H. Oncogenesis of T-ALL and nonmalignant consequences of overexpressing intracellular NOTCH1. *J. Exp. Med.* **205**, 2851–2861 (2008).
45. Stritesky, G. L., Jameson, S. C. & Hogquist, K. A. Selection of self-reactive T cells in the thymus. *Annu. Rev. Immunol.* **30**, 95–114 (2012).
46. Ben Baruch-Morgenstern, N. et al. Paired immunoglobulin-like receptor A is an intrinsic, self-limiting suppressor of IL-5-induced eosinophil development. *Nat. Immunol.* **15**, 36–44 (2014).
47. Adey, A. et al. Rapid, low-input, low-bias construction of shotgun fragment libraries by high-density in vitro transposition. *Genome Biol.* **11**, R119 (2010).

48. Jones, M. E. & Zhuang, Y. Acquisition of a functional T cell receptor during T lymphocyte development is enforced by HEB and E2A transcription factors. *Immunity* **27**, 860–870 (2007).
49. Wojciechowski, J., Lai, A., Kondo, M. & Zhuang, Y. E2A and HEB are required to block thymocyte proliferation prior to pre-TCR expression. *J. Immunol.* **178**, 5717–5726 (2007).
50. Winandy, S., Wu, L., Wang, J. H. & Georgopoulos, K. Pre-T cell receptor (TCR) and TCR-controlled checkpoints in T cell differentiation are set by Ikaros. *J. Exp. Med.* **190**, 1039–1048 (1999).

Acknowledgements

We thank H. Kawamoto (RIKEN Research Center for Allergy and Immunology) for reagents; M. Mandal for help with ATAC–seq; B. Kee, M. Clark, A. Khan, and A. Bendelac for advice; and M. Krishnan for helpful suggestions. This work was supported by National Institutes of Health grants R21AI076720, R01AI108682, and U54CA193419, and an ASH bridge grant (to F.G.), and R01CA160436 (to K.K). Further support came from the Chicago Biomedical Consortium (to F.G.) and UL1TR002003 (to M.M.-C.). A.O.E. was supported by an NIH minority supplement; P.S.M. was supported by Institutional NRSA T32 HL07605 and is currently supported as an LLS Fellow; J.Q. was supported by an AAI Careers in Immunology Fellowship; and M.K.O. is a T32HD007009 recipient.

Author contributions

A.O.E. designed and performed the experiments, interpreted the experiments, and wrote the manuscript; S.A., L.H., P.S.M., S.M., J.Q., and M.K.O. performed the experiments; M.M.-C. conducted and supervised bioinformatics analyses including the ATAC–seq bioinformatics; K.K. provided advice, interpreted the data, and helped write the manuscript; M.D. and F.G. designed and oversaw the study, interpreted the experiments, and wrote the manuscript.

Competing interests

The authors declare no competing interests.

Additional information

Supplementary information is available for this paper at https://doi.org/10.1038/s41590-018-0254-4.

Reprints and permissions information is available at www.nature.com/reprints.

Correspondence and requests for materials should be addressed to M.D. or F.G.

Publisher's note: Springer Nature remains neutral with regard to jurisdictional claims in published maps and institutional affiliations.

Methods

Mice. *Cd4*-Cre^{+}*Tcf7*$^{fl/-}$ (*Cd4*-Cre *Tcf7*$^{fl/-}$), *Cd4*-Cre^{+}*Tcf12*$^{fl/fl}$ (*Cd4*-Cre *Tcf12*$^{fl/fl}$), and littermate-control WT (*Cd4*-Cre^{+} or *Cd4*-Cre^{-}) mice were used in all experiments described. Mice were maintained on the C57BL/6 background, and experiments were performed with 6- to-8-week-old mice. Mice were housed in the animal facilities at the University of Chicago in accordance with protocol no. 71880, approved by the University of Chicago Institutional Animal Care and Use Committee.

BrdU uptake experiments. Mice were injected intraperitoneally with 1.8 mg of BrdU; 3 h later, the mice were euthanized, thymocytes were surface stained, and intracellular detection of BrdU incorporation was performed (with 8817-6600-42, eBioscience) according to the manufacturer's protocol.

Cell culture and inhibitor treatment. Thymocytes from WT, *Cd4*-Cre *Tcf7*$^{fl/-}$, and *Cd4*-Cre *Tcf12*$^{fl/fl}$ mice were labeled with fluorochrome-conjugated antibodies to CD4 (anti-CD4; 11-0042-82 eBiosciences) and CD8 (anti-CD8; 17-0081-82 eBiosciences) in flow cytometry buffer (2% FBS in PBS). DP thymocytes were sorted and cultured for 6 h with DMSO, 5 μg/ml MG-132 (m7449, Sigma), or 10 μg/ml DAPT (D5942, Sigma).

Flow cytometry and antibodies. Thymocytes from mice were surface stained in flow cytometry buffer (2% FBS in PBS) for 30 min on ice. Samples were washed with flow cytometry buffer, and data were acquired on an LSRII flow cytometer (Becton Dickinson). The data were analyzed with FlowJo software (Becton Dickinson). Antibodies were to CD4 (clone GK1.5, BD Biosciences), CD8 (clone 53-6.7, eBiosciences), TCRβ (clone H57-597, eBiosciences), and CD71 (clone R17217, BioLegend). A BrdU staining kit (8811-6600-42, eBiosciences) and live/dead kit (L34957, Molecular Probes) were also used. An annexin V PE kit (556422, BD Biosciences) was used to measure apoptosis according to the manufacturer's instructions.

Immunoblotting. Nuclear extracts from CD4^{+}CD8^{+} T cells were prepared with a Subcellular Protein Fractionation Kit (78840, Life Technologies) according to the manufacturer's instructions. Extracts were electrophoresed on a NuPAGE 4–12% Bis-Tris gel (NP0323, Invitrogen) and blotted. Membranes were probed with antibodies to TCF-1 (2203, Cell Signaling), HEB (SAB3500566, Sigma), and H3 (2650, Cell Signaling).

mRNA isolation. 1×10^7 CD4^{+}CD8^{+} T cells were sorted from three WT, *Tcf7*$^{fl/-}$, and *Cd4-Cre Tcf12*$^{fl/fl}$ mice each, and total RNA was isolated with TRIzol (15596026, Invitrogen) according to the protocol described by the Immunological Genome Project (https://www.immgen.org/). Libraries were generated and sequenced by the University of Chicago Genomics Facility.

Chromatin immunoprecipitation. 2×10^7 total thymocytes from 6- to 8-week-old mice were paraformaldehyde fixed at a final concentration of 1% (2106-01, J.T. Baker) for 15 min at room temperature (23 °C), quenched with glycine (0.125 M), and washed with ice-cold PBS containing protease inhibitors. Cells were resuspended in lysis buffer (10 mM Tris, pH 7.4, 1 mM EDTA, 1% Triton X-100, 0.1% sodium deoxycholate, 0.8 M NaCl, and 0.1% SDS) for 10 min at 4 °C and sonicated to an average size of 300 bp. Chromatin was incubated overnight with Protein G Dynabeads (10004D, Invitrogen) coupled to 5 μg of antibodies to TCF-1 (2203, Cell Signaling), HEB (SAB3500566, Sigma), Lef-1(2230, Cell Signaling), H3ac (06-599, Millipore), or H3K27ac (ab4729, Abcam). Protocols for Ikaros, H3K4me1, H3K4me2, H3K4me3, H3K27me3, and RNA Pol II were as previously described[35], as was that for Runx1 (ref. [51]). Beads were washed five times with lysis buffer (10 mM Tris, pH 7.4, 1 mM EDTA, 1% Triton X-100, 0.1% sodium deoxycholate, 0.5 M NaCl, and 0.1% SDS) and once with 1× TE. Chromatin was eluted with elution buffer (2% SDS and 20 mM Tris-HCl, pH 6.8) and reverse-cross-linked overnight at 65 °C. RNase A was added (50 μg/ml) and incubated at 37 °C for 1 h. Proteinase K was added to a final concentration of 240 μg/ml and incubated at 56 °C for 2 h. DNA was ethanol precipitated and resuspended in elution buffer (Qiagen).

Tcra rearrangements. DP thymocytes from mice were sorted, and RNA was extracted with TRIzol (15596026, Invitrogen) and treated with DNase. cDNA was synthesized with a SuperScript III kit (18080093, Invitrogen). Quantitative real-time PCR was performed to assess the abundance of *Tcra* rearrangements by using primers described previously[27].

Chromatin immunoprecipitation sequencing. ChIP material was prepared for sequencing in accordance with the Illumina/Solexa Genomic DNA protocol. Approximately 20 ng of immunoprecipitated DNA was end repaired, polyadenylated, ligated to Illumina TruSeq indexed adaptors, and purified with AMPure XP Beads (A63880, Beckman Coulter). Adaptor-ligated DNA was PCR amplified with KAPA Hifi DNA Polymerase (KK2601, Kapa Biosystems). PCR products were separated on a 2% agarose gel, and DNA fragments between 200 and 500 bp were excised and purified (28706, Qiagen). Libraries were sequenced on a HiSeq 4000 sequencer at the University of Chicago Genomics Facility.

Assay for transposase accessible chromatin and sequencing. 1×10^5 CD4^{+}CD8^{+} T cells sorted from WT, *Cd4*-Cre *Tcf7*$^{fl/-}$, and *Cd4*-Cre *Tcf12*$^{fl/fl}$ mice were used for ATAC–seq. Cells were centrifuged at 500 *g* at 4 °C for 5 min, washed with 1× PBS, and centrifuged again. Cells were resuspended in lysis buffer (10 mM Tris-HCl, pH 7.4, 10 mM NaCl, 3 mM $MgCl_2$, and 0.1% IGEPAL CA-630) and immediately centrifuged at 500 *g* at 4 °C for 10 min. Pellets were resuspended in transposition reaction buffer (25 μl 2× Tagment Buffer (FC-121-1030, Illumina), 2.5 μl Tagment DNA Enzyme, and 22.5 μl nuclease-free H_2O) for 30 min at 37 °C. DNA was purified with a Qiagen MinElute Kit and amplified with Nextera PCR primers (Illumina Nextera Index Kit) and NEBNext PCR Master Mix (M0541, New England BioLabs) for 11 cycles. Amplified DNA was purified with a Qiagen PCR cleanup kit. Libraries were sequenced on a HiSeq 4000 sequencer at the University of Chicago Genomics Facility.

Genome mapping and data analysis. Sequenced ChIP datasets were mapped with the Galaxy (https://usegalaxy.org/) suite of tools. Data were groomed and aligned to the mouse mm9 genome with Bowtie, allowing up to one mismatch and retaining only uniquely mapped reads, and unmapped reads were filtered. For transcription factors (TCF-1, HEB, Runx1, Ikaros, and Lef-1) peak calling was performed with MACS via HOMER[52]. Transcription-factor peak calling was performed relative to input controls with the requirement that peaks be at a minimum fivefold enriched over input and meet a *P*-value cutoff of 10×10^{-5}. Transcription-factor super-clusters were identified with HOMER's findPeaks command with the --style factor option, according to the strategy described by Whyte et al.[40]. This method combines transcription-factor peaks within a 12.5-kb region into a single cluster, then ranks these regions by score.

Sequenced RNA datasets were aligned to the mouse mm9 genome similarly to the ChIP–seq datasets. Differential expression analysis was performed with Cuffdiff 2 (ref. [53]). Genes with transcript abundance differences below $P < 0.05$ were considered to be significantly differentially expressed. Heat maps of normalized reads for gene subsets in WT, *Cd4*-Cre *Tcf7*$^{fl/-}$, and *Cd4*-Cre *Tcf12*$^{fl/fl}$ DP T cells were generated with the Cluster software.

Motif analysis was performed with HOMER's motif-discovery algorithm, and transcription-factor overlap analysis was conducted with HOMER's mergePeaks command, considering only peaks that directly overlapped. Peaks were annotated to the mm9 genome with annotatePeaks.pl in HOMER. Histograms for transcription factors and histone modifications were generated with NGS. PLOT software[54]. *K*-means clustering of ChIP–seq datasets and heat maps was also generated with NGS.PLOT.

Transcription-factor binding and nucleosome positioning were visualized with the Integrated Genome Browser software[55]. Pathway enrichment analysis for genes identified by ChIP–seq and RNA-seq analysis was performed via Metascape (http://metascape.org)[56].

ATAC–seq peak analysis. *Peak calling.* Read alignments were first adjusted to account for TAC transposon binding: + 4 bp for positive-strand alignments and −5 bp for negative-strand alignments. The open-chromatin enrichment track was generated by creating a bedGraph from the raw reads with bedtools genomcov[57] and was then converted to bigWig with the UCSC tool bedGraphToBigWig[58]; tracks were normalized by the sum of alignment lengths greater than 1 billion. The start-position track was generated by taking just the first base of the alignment for positive-strand alignments or the last base of the alignment for negative-strand alignments, then creating bedGraph and bigWig tracks as for the open chromatin; tracks were normalized to the alignment count greater than 1 million. Open-chromatin peaks were called with Macs2 (ref. [59]) with --nomodel set and no background provided; peaks with a score >5 were retained.

Nucleosome positioning. Properly paired read pairs were first placed into nucleosome-free or nucleosome-containing bins, on the basis of their fragment size. Fragments ≤ 100 bp were considered nucleosome free (background) and converted to a single read covering the length of the fragment. Fragments 180–247 bp were considered single-nucleosome containing and were converted to a single read the length of the fragment; similarly, fragments 315–473 bp or 558–615 bp were considered to contain two or three nucleosomes, and were split into two or three reads covering one-half or one-third of the total fragment length. Single-, two-, and three- nucleosome reads were combined into the nucleosome-signal read set. Nucleosome positioning analysis was run with danpos[60] with command depose and parameters -m 1 -a 10 -jd 20 --clonalcut 0, and contrasting nucleosome signal to nucleosome background for each sample. Wig tracks from danpos were renormalized to counts per billion bases with the sum of alignment lengths greater than 1 billion from the original BAM file, then converted to bigWig with the UCSC tool wigToBigWig[58].

Nucleosome quantification. Nucleosome presence or absence was determined with the UCSC tool bigWigAverageOverBed (https://genome.ucsc.edu/). Nucleosome occupancy was scored over genomic regions representing TCF-1- and HEB-

binding sites, and reported as confidence scores. Negative values indicated the absence of nucleosomes, whereas positive values represented an increased likelihood of the presence of a nucleosome at each region.

Density plots (Spearman correlation). Density plots were created with the stat_bin2d function in the ggplot2 package in R, with 30 bins in each dimension. For visualization purposes, the axis ranges of some density plots were limited to highlight the high-probability regions of the plot.

Spearman correlation coefficients and *P* values were computed in R with the cor and cor.test functions.

Statistical analysis. Results from biologically distinct experiments were combined and analyzed with the indicated statistical tests in Prism 7 (GraphPad). The statistical significance of RNA-seq data was determined with Cuffdiff. ChIP–seq (factor enrichment) and ATAC–seq (chromatin accessibility) *P*-value cutoffs were determined with MACS2. Gene pathway enrichment *P* values were determined with Metascape. Nucleosome-occupancy statistical tests were calculated in R. Data are presented as mean ± s.d. unless stated otherwise.

Reporting Summary. Further information on research design is available in the Nature Research Reporting Summary linked to this article.

Data availability

Sequencing data supporting the findings of this study have been deposited in the Sequence Read Archive (SRA) database under SRA accession number SRP142342. All other relevant data are available from the corresponding authors upon reasonable request.

References

51. Huang, H. et al. Differentiation-dependent interactions between RUNX-1 and FLI-1 during megakaryocyte development. *Mol. Cell. Biol.* **29**, 4103–4115 (2009).
52. Heinz, S. et al. Simple combinations of lineage-determining transcription factors prime cis-regulatory elements required for macrophage and B cell identities. *Mol. Cell* **38**, 576–589 (2010).
53. Trapnell, C. et al. Differential gene and transcript expression analysis of RNA-seq experiments with TopHat and Cufflinks. *Nat. Protoc.* **7**, 562–578 (2012).
54. Shen, L., Shao, N., Liu, X. & Nestler, E. ngs.plot: quick mining and visualization of next-generation sequencing data by integrating genomic databases. *BMC Genomics* **15**, 284 (2014).
55. Freese, N. H., Norris, D. C. & Loraine, A. E. Integrated genome browser: visual analytics platform for genomics. *Bioinformatics* **32**, 2089–2095 (2016).
56. Tripathi, S. et al. Meta- and orthogonal Integration of Influenza "OMICs" data defines a role for UBR4 in virus budding. *Cell Host Microbe* **18**, 723–735 (2015).
57. Quinlan, A. R. & Hall, I. M. BEDTools: a flexible suite of utilities for comparing genomic features. *Bioinformatics* **26**, 841–842 (2010).
58. Kent, W. J., Zweig, A. S., Barber, G., Hinrichs, A. S. & Karolchik, D. BigWig and BigBed: enabling browsing of large distributed datasets. *Bioinformatics* **26**, 2204–2207 (2010).
59. Zhang, Y. et al. Model-based analysis of ChIP-Seq (MACS). *Genome Biol.* **9**, R137 (2008).
60. Chen, K. et al. DANPOS: dynamic analysis of nucleosome position and occupancy by sequencing. *Genome Res.* **23**, 341–351 (2013).

nature research

Corresponding author(s): Fotini Gounari, Marei Dose.

Reporting Summary

Nature Research wishes to improve the reproducibility of the work that we publish. This form provides structure for consistency and transparency in reporting. For further information on Nature Research policies, see Authors & Referees and the Editorial Policy Checklist.

Statistical parameters

When statistical analyses are reported, confirm that the following items are present in the relevant location (e.g. figure legend, table legend, main text, or Methods section).

n/a	Confirmed	
☐	☒	The exact sample size (*n*) for each experimental group/condition, given as a discrete number and unit of measurement
☐	☒	An indication of whether measurements were taken from distinct samples or whether the same sample was measured repeatedly
☐	☒	The statistical test(s) used AND whether they are one- or two-sided *Only common tests should be described solely by name; describe more complex techniques in the Methods section.*
☐	☒	A description of all covariates tested
☐	☒	A description of any assumptions or corrections, such as tests of normality and adjustment for multiple comparisons
☐	☒	A full description of the statistics including central tendency (e.g. means) or other basic estimates (e.g. regression coefficient) AND variation (e.g. standard deviation) or associated estimates of uncertainty (e.g. confidence intervals)
☐	☒	For null hypothesis testing, the test statistic (e.g. *F*, *t*, *r*) with confidence intervals, effect sizes, degrees of freedom and *P* value noted *Give P values as exact values whenever suitable.*
☒	☐	For Bayesian analysis, information on the choice of priors and Markov chain Monte Carlo settings
☐	☒	For hierarchical and complex designs, identification of the appropriate level for tests and full reporting of outcomes
☒	☐	Estimates of effect sizes (e.g. Cohen's *d*, Pearson's *r*), indicating how they were calculated
☐	☒	Clearly defined error bars *State explicitly what error bars represent (e.g. SD, SE, CI)*

Our web collection on statistics for biologists may be useful.

Software and code

Policy information about availability of computer code

Data collection	No software was used for data collection.
Data analysis	HOMER, MACS2, bigWigAverageOverBed, wigToBigWig, FlowJo, Prism, R, Cuffdif, NGSPLOT, BETA, Metascape, Cluster, and Integrated Genome Browser were used for data analysis and visualization.

For manuscripts utilizing custom algorithms or software that are central to the research but not yet described in published literature, software must be made available to editors/reviewers upon request. We strongly encourage code deposition in a community repository (e.g. GitHub). See the Nature Research guidelines for submitting code & software for further information.

Data

Policy information about availability of data

All manuscripts must include a data availability statement. This statement should provide the following information, where applicable:

- Accession codes, unique identifiers, or web links for publicly available datasets
- A list of figures that have associated raw data
- A description of any restrictions on data availability

RNA-seq, ChIP-seq and ATAC-seq data sets have been deposited in the GEO database with accession code SRP142342.

Field-specific reporting

Please select the best fit for your research. If you are not sure, read the appropriate sections before making your selection.

☒ Life sciences ☐ Behavioural & social sciences ☐ Ecological, evolutionary & environmental sciences

For a reference copy of the document with all sections, see nature.com/authors/policies/ReportingSummary-flat.pdf

Life sciences study design

All studies must disclose on these points even when the disclosure is negative.

Sample size	Sample size was chosen according to standard practices in the field. ChIP-seq and ATAC-seq samples were prepared in duplicate. RNA-seq samples were prepared in triplicates. All biochemical experiments were performed 2~5 as described in figure legends. No statistical methods were used to predetermine sample sizes.
Data exclusions	No data were excluded.
Replication	All biochemical and flow cytometry experiments were replicated as described in figure legends. All replicated data were analyzed for statistical significance.
Randomization	Samples were grouped by genotype. No randomization was performed.
Blinding	No blinding was performed in this study.

Reporting for specific materials, systems and methods

Materials & experimental systems

n/a	Involved in the study
☒	☐ Unique biological materials
☐	☒ Antibodies
☒	☐ Eukaryotic cell lines
☒	☐ Palaeontology
☐	☒ Animals and other organisms
☒	☐ Human research participants

Methods

n/a	Involved in the study
☐	☒ ChIP-seq
☐	☒ Flow cytometry
☒	☐ MRI-based neuroimaging

Antibodies

Antibodies used	CD4 (clone GK1.5, BD Biosciences), CD8 (clone 53-6.7, eBiosciences), TCRB (clone H57-597, eBiosciences), CD71 (clone R17217, BioLegend), Live/dead (L34957, Molecular Probes), BrdU (8811-6600-42, eBiosciences), and Annexin-V PE kit (556422, BD Biosciences).
Validation	Antibodies were validated by manufacturer.

Animals and other organisms

Policy information about studies involving animals; ARRIVE guidelines recommended for reporting animal research

Laboratory animals	Thymocytes and thymocyte subsets were isolated from 6-8 week old male or female mice in the C57BL/6 background
Wild animals	No wild animals were used in this study.
Field-collected samples	No field-collected samples were used int his study.

ChIP-seq

Data deposition

☒ Confirm that both raw and final processed data have been deposited in a public database such as GEO.

☐ Confirm that you have deposited or provided access to graph files (e.g. BED files) for the called peaks.

Data access links *May remain private before publication.*	Data have been submitted and can be accessed upon publication at https://www.ncbi.nlm.nih.gov/sra/SRP142342
Files in database submission	*Provide a list of all files available in the database submission.*
Genome browser session (e.g. UCSC)	*Provide a link to an anonymized genome browser session for "Initial submission" and "Revised version" documents only, to enable peer review. Write "no longer applicable" for "Final submission" documents.*

Methodology

Replicates	Biological replicates were submitted for each ChIP-seq, RNA-seq, and ATAC-seq samples.
Sequencing depth	For ChIP-seq and RNA-seq datasets 30-50 million raw reads were sequenced. Samples were sequenced as 50bp single end reads. ATAC-seq samples were sequenced to a depth of ~100 million reads and sequenced as 50bp paired end reads. RNA-seq samples were sequenced to a depth of 50-60 million reads and sequenced as 50bp single end reads.
Antibodies	anti-H3K4me3 (Abcam ab8580 or Millipore 07-473), anti-H3K4me2 (Millipore 07-030), anti-H3K4me1 (Abcam ab8895), anti-H3Ac (Millipore 06-599), anti-H3K27me3 (Millipore 07-449), anti-RNA polII S5 (Abcam ab5131), anti-TCF1/Tcf7 (Cell Signaling, C63D9 (2203)), anti-HEB/Tcf12 (Sigma, SAB3500566), anti-Lef1 (Cell Signaling, 2230),.
Peak calling parameters	Transcription factor peaks were called using HOMER with a requirement that peaks occurred at a fold over input = 5.00 and poisson p-value over local region required = 1.00 e-05. ATAC-seq peaks were called using MACS2 to identify broad regions using default mfold (5,50) and a poisson p-value over local region of 1.00 e-05.
Data quality	Fold over local region required = 5.00 and Poisson p-value over local region required = 1.00e-05. FASTQC was used to ensure maximum per base sequence quality of sequenced data.
Software	Short reads were aligned to the mouse reference genome (mm9) using the Bowtie 2. Reads with multiple alignments were removed with samtools (v1.1). To identify peaks from ChIP-seq reads, we used the HOMER package makeTagDirectory followed by the findPeaks command with the 'factor' parameter. ATAC-seq peaks were identified using MACS2. NGSPLOT was used to k-means cluster ChIP-seq datasets and visualize factor enrichment. Cuffdiff was used to analyze RNA-seq data. BETA was used to merge ChIP-seq and RNA-seq data.

Flow Cytometry

Plots

Confirm that:

☒ The axis labels state the marker and fluorochrome used (e.g. CD4-FITC).

☒ The axis scales are clearly visible. Include numbers along axes only for bottom left plot of group (a 'group' is an analysis of identical markers).

☒ All plots are contour plots with outliers or pseudocolor plots.

☒ A numerical value for number of cells or percentage (with statistics) is provided.

Methodology

Sample preparation	Thymi were gently dissociated into FACS buffer (2%FBS) using fully frosted microscope slides, passed through 40uM filters, and stained for indicated markers.
Instrument	LSR Fortessa, BD FACSAriaII
Software	Flowjo was used for data analysis and BD FACSDiva was used for data acquisition.
Cell population abundance	CD4CD8 double positive cells were FACS purified around 95% purity by double sorting.
Gating strategy	Starting cells were gated by FSC/SSC gates and then on live/dead stain to select live populations.

☐ Tick this box to confirm that a figure exemplifying the gating strategy is provided in the Supplementary Information.